



A cut finite-element method for fracture and contact problems in large-deformation solid mechanics

Michael Poluektov^{a,*}, Łukasz Figiel^{a,b}

^a *International Institute for Nanocomposites Manufacturing, WMG, University of Warwick, Coventry CV4 7AL, UK*

^b *Warwick Centre for Predictive Modelling, University of Warwick, Coventry CV4 7AL, UK*

Received 17 May 2021; received in revised form 24 September 2021; accepted 8 October 2021

Available online 11 November 2021

Abstract

Cut finite-element methods (CutFEMs) belong to the class of methods that allow boundaries/interfaces to cut through the elements, which avoids any meshing/remeshing problems. This is highly convenient from a practical point of view, especially when non-stationary interfaces are considered, e.g. phase boundaries in solids, as the interfaces can move independently of the mesh. There are many research directions related to CutFEM, one of which focuses on the equations of solid mechanics. Initially, the developments centred on linear elasticity and, in the previous publication by the authors, the method has been extended to large deformations and arbitrary constitutive relations, while the focus has been on phase boundaries in solids and on localised chemical reaction fronts in coupled mechanics–diffusion–reaction systems. In this paper, the method is further extended to more complex physics of the interfaces — fracture, i.e. separation of the interface into two surfaces in the current configuration, and contact between the separated surfaces. Several cases are considered — fracture with linear and non-linear traction separation, contact without and with adhesion. Each incremental generalisation of the approach contains a prior approach as a particular case, e.g. the phase boundary problem is a particular case of the fracture problem. The contact problem is treated in an unbiased way — the weak form is symmetric with respect to the choice of the contact surfaces for the integration. The weak forms are derived from the total energy functional. The proposed method has been tested computationally for the case of linear elements and passed the so-called patch tests and the convergence rate tests demonstrating the asymptotically optimal rates.

© 2021 The Author(s). Published by Elsevier B.V. This is an open access article under the CC BY-NC-ND license (<http://creativecommons.org/licenses/by-nc-nd/4.0/>).

Keywords: Cut finite element method; Fictitious domain method; Sharp interface method; Contact mechanics; Large deformation mechanics; Unbiased contact formulation

1. Introduction

Solving PDEs defined on domains with interfaces still remains one of the challenging problems in computational sciences, especially when physics of these interfaces is non-trivial and involves a coupling between a number of physical processes. Non-stationary interfaces represent a specific challenge for computational techniques, while solution of such problems is highly relevant for physical sciences. These problems are encountered in a large variety

* Corresponding author.

E-mail address: m.poluektov@warwick.ac.uk (M. Poluektov).

of applications, e.g. two-phase flows, fluid–structure interactions, phase transitions, diffusion–reaction systems, fracture and damage in solids, etc.

One of the ways of handling interfaces that gained significant popularity in recent years is the class of fictitious-domain methods, also called non-conforming mesh methods or unfitted methods. In this approach, the computational mesh is independent of the geometry, the interfaces can arbitrarily cut through the elements and, in the case of non-stationary problems, can move independently of the mesh. The advantages of such approach are obvious — it not only completely avoids remeshing for non-stationary interfaces, but it is also useful for stationary problems with complex interface geometries and allows using structured meshes.

One of such methods is the cut finite-element method or CutFEM [1,2]. Literature on CutFEM is vast and this introduction does not aim to be exhaustive. It is important to mention that the method originates from [3], where it has been proposed to use the Nitsche’s method [4] to enforce the boundary/interface conditions, and from [1], where the numerical stabilisation has been proposed. For a summary of the method, the reader is referred to overview [2] and references therein. The subsequent research includes the improvement of the quadrature on cut elements, e.g. [5], further development of the method for PDEs on surfaces and on embedded manifolds in general, e.g. [6–8], generalisation of the numerical stabilisation, e.g. [9], formulation of the space–time FEM with cut elements, e.g. [10,11], tailoring the method to specific applications such as topology optimisation [12,13].

Perhaps the most well-known (in the computational mechanics community) unfitted method for interface problems is XFEM/GFEM [14–16]; therefore, it is important to highlight its relation to CutFEM. The main idea of the XFEM framework is the enrichment of the numerical solution, such that it becomes a sum of the standard finite-element approximation and products of some enrichment functions, partition of unity functions [17] and additional degrees of freedom. Taking a crack opening as an example of an interface problem, the enrichment is typically done locally for the elements that are cut by the crack, the enrichment function is typically taken to be the Heaviside step function for the elements containing the crack surface and taken to be an asymptotic solution for the elements containing the crack tip [16,18]. For the phase boundary problems, the enrichment function has initially been proposed to be the ridge function [19–21], i.e. the absolute value of the level set function defining the interface, but it can also be the Heaviside step function [22,23]. In the CutFEM method, the elements that are cut by the crack have doubled degrees of freedom [3,24], i.e. an extra element is added for every cut element, which is a form of enrichment of the numerical solution. Such enrichment can be derived from the standard XFEM, as has been shown in detail in Section 3.2.1 of Ref. [18].

For most types of interfaces, there is a need to enforce specific interface conditions, which is done via the weak form. For cohesive cracks treated within the XFEM framework, it has been proposed to account for additional cohesive forces within the principle of virtual work (or virtual power) as work of tractions on virtual displacements at both sides of the crack [25–28]. For phase boundaries treated within the XFEM framework, various enforcement techniques of the interface conditions exist: one option is to use the ridge function for the solution enrichment and the standard weak form [21], an alternative option is to use the Heaviside function for the solution enrichment and impose the interface conditions via the Lagrange multipliers [22,23]. The latter approach is similar to the enforcement of the interface conditions using the Nitsche’s method, as has been discussed in [23]. As described earlier, the CutFEM framework uses the Nitsche’s method [2]; therefore, it might be viewed as a particular case of the XFEM framework. According to the best knowledge of the authors, in the numerical analysis community, name ‘CutFEM’ consolidated for a non-conforming mesh framework relying on (a) the Nitsche’s method for enforcement of the boundary/interface conditions and (b) using a some form of inter-element stabilisation for cut elements (or ghost penalty) as introduced in [1].

Within the area of solid mechanics, CutFEM without inter-element stabilisation has originally been formulated for linear elasticity problems in [24] and the stabilised version of CutFEM for linear elasticity has been proposed in [29]. It is also noteworthy to mention an overview paper on elasticity and interfaces [30]. The method has been extended to non-linear problems of solid mechanics (i.e. large deformations and arbitrary constitutive relations) in [31], where not only phase boundaries in solids have been considered, but also more general localised chemical reaction fronts (or transformation fronts) in coupled mechanics–diffusion–reaction systems. The extension, however, has been limited to interfaces without damage, i.e. without separation between surfaces belonging to different subdomains. Although fracture problems have been considered in the original paper [24], they were limited to linear elasticity. Therefore, the first aim of this paper is to extend the CutFEM approach to fracture problems in large-deformation solid mechanics.

In fracture problems, the initial interface in the reference configuration splits into two surfaces in the current configuration, and, when large deformations are considered, these surfaces can come in contact. Furthermore, in large deformations, the images of the contact points in the reference configuration can be significantly distanced. This requires proper resolution of the contact conditions. The idea of the Nitsche's method, which is used in CutFEM, has also been applied to contact problems in solid mechanics. Originally, the Nitsche-based contact resolution has been formulated for linear elastic contact problems [32] and then extended to large deformations [33], based on the earlier results of [34,35], and even to coupled problems such as thermo-mechanics [36]. Thus, the second aim of this paper is to incorporate the Nitsche-based resolution of the contact conditions at the interface into CutFEM.

2. Numerical method

The presentation of the generalisation of the CutFEM approach for fracture and contact problems in large-deformation solid mechanics is split in four major parts. In the first part, the general framework for interface problems is summarised. The second part deals with the case of phase boundary in solids (e.g. a discontinuity in constitutive relations) and summarises some results from [31]. In the third and the fourth parts, the fracture and the contact problems are considered, respectively.

The major goal here is twofold. The first goal is to ensure that any incremental generalisation of the approach contains a prior approach as a particular case, i.e. the phase boundary problem is a particular case of the fracture problem, while the latter can become a particular case of the contact problem under some conditions. The second goal is to ensure that the weak form obtained for the contact problem is symmetric with respect to the choice of the contact surfaces for the integration, i.e. the weak form contains integrals over both surfaces that come into contact and the integrals corresponding to the first surface have the same structure as the integrals corresponding to the second surface.

2.1. General interface problem

2.1.1. Problem formulation

The solid body is split into two subdomains, which are separated by an interface. A static problem is considered, i.e. there are no dynamic terms in the linear momentum balance equations. The problem is to find the deformed state of the material under a certain load by solving the linear momentum balance equation:

$$\nabla \cdot \boldsymbol{\sigma}_{\pm} = \vec{0}, \quad \vec{x} \in \omega_{\pm}. \quad (1)$$

Here, the same tensor notation as in the previous publication by the authors is used [31]. Current position vector \vec{x} of a material point is a function of position vector \vec{X} of the point in the reference configuration. Nabla operators ∇_0 and $\nabla = \mathbf{F}^{-T} \cdot \nabla_0$ are defined with respect to the reference and the current configurations, respectively, where \mathbf{F} is the deformation gradient, which maps the reference configuration to the current configuration: $\mathbf{F} = (\nabla_0 \vec{x})^T$. The Cauchy stress tensor is denoted as $\boldsymbol{\sigma}$. Quantities (deformation gradients, stresses, displacements, etc.) corresponding to subdomains one and two are denoted with subscripts '+' and '-', respectively. As seen from Eq. (1), to shorten the description, subscript '±' is used on some occasions to combine two separate equations corresponding to two subdomains into one equation. In the current configuration, subdomains one and two are denoted as ω_+ and ω_- , respectively. These domains are separated by interface γ_* . The normal to γ_* is denoted as \vec{n}_* and is defined as the outer normal to ω_+ . Mappings of ω_+ and ω_- onto the reference configuration are denoted as Ω_+ and Ω_- , respectively. These subdomains are separated by interface Γ_* . The normal to the interface is defined as the outer normal to Ω_+ and is denoted as \vec{N}_* .

The outer boundary of the body is split into γ_D and γ_T , on which displacements and tractions are enforced, respectively. The normal to γ_T is denoted as \vec{n}_T and is defined as the outer normal to the body. The boundary conditions at the outer surface of the body can be written as

$$\vec{u}_{\pm} = \vec{d}, \quad \vec{x} \in \gamma_{D\pm}, \quad \gamma_{D\pm} = \gamma_D \cap \partial\omega_{\pm}, \quad (2)$$

$$\boldsymbol{\sigma}_{\pm} \cdot \vec{n}_T = \vec{t}, \quad \vec{x} \in \gamma_{T\pm}, \quad \gamma_{T\pm} = \gamma_T \cap \partial\omega_{\pm}, \quad (3)$$

where \vec{u} is the displacement of a material point, \vec{d} is the imposed displacement vector and \vec{t} is the imposed traction vector. There are of course interface conditions enforced at γ_* , which are considered below separately for each problem.

It is also useful to rewrite the boundary conditions with respect to the reference configuration. Here, Γ_D and Γ_T are the images of γ_D and γ_T , respectively, in the reference configuration. The normal to Γ_T is denoted as \vec{N}_T and is defined as the outer normal to the body. Then, the boundary conditions at the outer surface of the body can be written as

$$\vec{u}_\pm = \vec{d}, \quad \vec{X} \in \Gamma_{D\pm}, \quad \Gamma_{D\pm} = \Gamma_D \cap \partial\Omega_\pm, \tag{4}$$

$$\mathbf{P}_\pm \cdot \vec{N}_T = \vec{T}, \quad \vec{X} \in \Gamma_{T\pm}, \quad \Gamma_{T\pm} = \Gamma_T \cap \partial\Omega_\pm, \tag{5}$$

where \mathbf{P} is the first Piola–Kirchhoff stress tensor and \vec{T} is the imposed traction defined per unit surface in the reference configuration. As usual, for the purpose of presenting a numerical method, \vec{T} is assumed to be independent of displacement \vec{u} ; however, it is easy to construct the generalisation. In the reference configuration, the interface conditions are enforced at Γ_* .

Only one assumption is made regarding the constitutive relations — the materials have a defined strain energy density such that

$$\mathbf{P} = \frac{\partial W}{\partial \mathbf{F}}, \tag{6}$$

where W is the strain energy density per unit volume in the reference configuration. It should be emphasised that such assumption is valid not only for hyperelasticity but also for a larger range of material models, for example, for the so-called hyperelastoplasticity.¹

2.1.2. Method

The weak form of the linear momentum balance equation, which is required for the finite-element discretisation, can be obtained either from the strong form or by variation of the total energy. Here, the latter route is chosen. The total energy can be represented by four terms:

$$\Pi = \Pi_+ + \Pi_- + \Pi_* + \Pi_I, \tag{7}$$

where Π_+ and Π_- are the bulk energies corresponding to subdomains one and two, respectively, Π_* is the energy corresponding to the interface, Π_I is the inter-element stabilisation energy that is usually introduced in the CutFEM methods and is considered in Section 2.5. At this point, a general interface is considered and later, different energies are specified for different types of the interface (phase boundary, crack opening, contact). The energies of the subdomains are trivially expressed as

$$\Pi_\pm = \int_{\Omega_\pm} W_\pm \, d\Omega_\pm - \int_{\Gamma_{T\pm}} \vec{u}_\pm \cdot \vec{T} \, d\Gamma_{T\pm}. \tag{8}$$

The variation of the bulk energies can be obtained in the straightforward way:

$$\delta\Pi_\pm = \int_{\Omega_\pm} \mathbf{P}_\pm : \nabla_0 \vec{\varphi}_\pm \, d\Omega_\pm - \int_{\Gamma_{T\pm}} \vec{\varphi}_\pm \cdot \vec{T} \, d\Gamma_{T\pm}, \tag{9}$$

where $\vec{\varphi}_\pm = \delta\vec{u}_\pm$ is introduced. Although it is easy to see how (9) emerges from Eqs. (6) and (8), a more detailed explanation is available in [31].

To ensure that the functions under the integrals are integrable, the following functional spaces are introduced:

$$\mathcal{R}_\pm = \left\{ \vec{u} \mid u_i \in H^1(\Omega_\pm), \vec{u} = \vec{d} \text{ on } \Gamma_{D\pm} \right\}, \quad u_i = \vec{u} \cdot \vec{e}_i, \quad i \in \{1, 2, 3\}, \tag{10}$$

¹ For example, when the rheological model of the material consists of two sequential elements: elastic and purely plastic, the deformation gradient is decomposed as $\mathbf{F} = \mathbf{F}_e \cdot \mathbf{F}_p$, while the stresses in the elastic element are equal to the stresses in the plastic element and are equal to the total stresses $\boldsymbol{\sigma} = \boldsymbol{\sigma}_e$. Assuming that there is strain energy density $W_e = W_e(\mathbf{F}_e)$ of the elastic element, it can be written that $\mathbf{P}_e = J_e \boldsymbol{\sigma}_e \cdot \mathbf{F}_e^{-T} = \partial W_e / \partial \mathbf{F}_e$, where $J_e = \det(\mathbf{F}_e)$. Considering an isochoric plasticity model ($J = J_e$), it follows that

$$\begin{aligned} \mathbf{P} &= J \boldsymbol{\sigma} \cdot \mathbf{F}^{-T} = J_e \boldsymbol{\sigma}_e \cdot \mathbf{F}_e^{-T} \cdot \mathbf{F}_p^{-T} = \frac{\partial W_e}{\partial \mathbf{F}_e} \cdot \mathbf{F}_p^{-T} = \frac{\partial W_e}{\partial \mathbf{F}_e} : \left(\mathbf{F}_p^{-T} \cdot \mathbf{4}\mathbf{I} \right) = \frac{\partial W_e}{\partial \mathbf{F}_e} : \left(\mathbf{F}_p^{-T} \cdot \frac{\partial \mathbf{F}^T}{\partial \mathbf{F}} \right) = \\ &= \frac{\partial W_e}{\partial \mathbf{F}_e} : \frac{\partial \mathbf{F}_e^T}{\partial \mathbf{F}} = \frac{\partial W_e}{\partial \mathbf{F}}. \end{aligned}$$

$$\mathcal{Q}_\pm = \left\{ \vec{\varphi} \mid \varphi_i \in H^1(\Omega_\pm), \vec{\varphi} = \vec{0} \text{ on } \Gamma_{D\pm} \right\}, \quad \varphi_i = \vec{\varphi} \cdot \vec{e}_i, \quad i \in \{1, 2, 3\}. \tag{11}$$

Here, u_i are components of vector function \vec{u} and $H^1(\Omega_\pm)$ is the Sobolev space with the L^2 -norm. The resulting weak problem formulation is the following:

$$\text{find } \vec{u}_+ \in \mathcal{R}_+, \vec{u}_- \in \mathcal{R}_- \text{ such that } a(\vec{u}_+, \vec{u}_-, \vec{\varphi}_+, \vec{\varphi}_-) = 0, \quad \forall \vec{\varphi}_+ \in \mathcal{Q}_+, \forall \vec{\varphi}_- \in \mathcal{Q}_-,$$

where

$$a(\vec{u}_+, \vec{u}_-, \vec{\varphi}_+, \vec{\varphi}_-) = \delta\Pi_+ + \delta\Pi_- + \delta\Pi_* + \delta\Pi_I. \tag{12}$$

Term $\delta\Pi_*$ is the variation of the interfacial energy and is considered separately for different interface problems. Term $\delta\Pi_I$ is the variation of the stabilisation energy and is given in Section 2.5.

After the weak form is obtained, a finite-element mesh must be introduced, as well as the standard nodal basis functions. Following the finite-element formulation, the system of non-linear algebraic equations with respect to the unknown nodal degrees of freedom must be assembled. These two steps are rather straightforward and have been outlined many times in literature, e.g. in Sections 4.1.4 and 4.1.5 of Ref. [31]. Therefore, the summary of the finite-element formulation of the problem is given in Appendix.

2.2. Phase boundary

2.2.1. Problem formulation

In the phase boundary problem, two subdomains correspond to two different phases of the material and can have different constitutive behaviour. Within the theory of solid–solid phase transitions, three different configurations are usually introduced — the current configuration, the reference configuration of phase one and the reference configuration of phase two. A transformation strain then links the reference configurations of the phases. However, numerically, the problem is solved only in one given configuration; therefore, for the purposes of this paper, it is sufficient to consider only one reference configuration, e.g. the reference configuration of phase ‘-’, and assume that the phases can have different constitutive laws.² More detailed discussion of the configurations for this case can be found in [31] and references therein.

For the phase boundary problem, the displacement and the traction continuity conditions are enforced at the interface. In the current configuration, these conditions are written as

$$\vec{u}_- = \vec{u}_+, \quad \vec{x} \in \gamma_*, \tag{13}$$

$$\boldsymbol{\sigma}_- \cdot \vec{n}_* = \boldsymbol{\sigma}_+ \cdot \vec{n}_*, \quad \vec{x} \in \gamma_*, \tag{14}$$

and in the reference configuration, these conditions become

$$\vec{u}_- = \vec{u}_+, \quad \vec{X} \in \Gamma_*, \tag{15}$$

$$\mathbf{P}_- \cdot \vec{N}_* = \mathbf{P}_+ \cdot \vec{N}_*, \quad \vec{X} \in \Gamma_*. \tag{16}$$

It is also useful to introduce brackets $[[\cdot]]_*$ to denote the jump of the quantity across the interface and brackets $\langle \cdot \rangle$ to denote the average of the quantity across the interface.³

The problem consists in solving Eq. (1) with corresponding boundary conditions (4), (5) enforced at the external boundary of the body and interface conditions (15), (16).

2.2.2. Method

For the case when the interface is the phase boundary, the following interfacial energy is introduced [31]:

$$\Pi_*^B = \int_{\Gamma_*} \left(\frac{1}{2} \frac{\lambda}{h} [[\vec{u}]]_* - \langle \mathbf{P} \rangle \cdot \vec{N}_* \right) \cdot [[\vec{u}]]_* d\Gamma_*, \tag{17}$$

² For example, an illustrative analogy of this approach can be finding a deformed state of a body, one half of which is exactly at temperature 0 °C, while the other half is exactly at 100 °C. There is a stress-free configuration of the body, when the entire volume is at 0 °C, and a stress-free configuration, when the entire volume is at 100 °C. The problem can be solved in the first configuration, prescribing a constitutive law for the second half of the body to contain a thermal expansion by 100 °C.

³ For example, $\langle \mathbf{P} \rangle = (\mathbf{P}_+ + \mathbf{P}_-)/2$ and $[[\vec{u}]]_* = \vec{u}_+ - \vec{u}_-$.

where h is the typical mesh size and λ is the penalty parameter. The first term is explained below. The second term is obtained from writing the work of tractions at the interface (analogous to the second term of (8)) for subdomains ‘+’ and ‘-’ separately and combining them together using the continuity of tractions interface condition. Eq. (17) is a version of the augmented Lagrangian approach, which is sometimes used to derive the Nitsche’s method if the traction is interpreted as a multiplier [37].

The variation of Π_*^B results in

$$\delta\Pi_*^B = \int_{\Gamma_*} \left(\frac{\lambda}{h} \llbracket \vec{u} \rrbracket_* \cdot \llbracket \vec{\varphi} \rrbracket_* - \langle \mathbf{P} \rangle : \vec{N}_* \llbracket \vec{\varphi} \rrbracket_* - \llbracket \vec{u} \rrbracket_* \vec{N}_* : \left\langle \frac{\partial \mathbf{P}^T}{\partial \mathbf{F}} : \nabla_0 \vec{\varphi} \right\rangle \right) d\Gamma_*, \tag{18}$$

which results in weak form (12) with the following interfacial term:

$$\text{for phase boundary problem } \delta\Pi_* = \delta\Pi_*^B.$$

It can be seen that the first term in (17) resulted in the term containing $\llbracket \vec{u} \rrbracket_* \cdot \llbracket \vec{\varphi} \rrbracket_*$, which is usually introduced in the numerical frameworks with the enforcement of the boundary conditions using the Nitsche-type methods [3] to ensure the coercivity of the weak form. In [31], it has been additionally shown that such weak form of the problem, Eq. (12) with $\delta\Pi_* = \delta\Pi_*^B$ and without stabilisation term $\delta\Pi_1$, can equivalently be obtained directly from the strong form of the problem, Eq. (1) with boundary conditions (4), (5) and interface conditions (15), (16).

2.3. Crack opening

2.3.1. Problem formulation

From the mathematical point of view, the problem formulation for the fracture is somewhat similar to the problem formulation for the phase boundary. However, now, the separation of the boundaries in the current configuration is allowed, i.e. $\llbracket \vec{u} \rrbracket_*$ can be non-zero. When a typical matrix-inclusion problem is considered, there are two phases (the matrix and the inclusion) and an interface between them. If a discrete crack is considered with a crack tip located in the bulk, formally, there is only one phase; however, it is still necessary to distinguish between two surfaces that separate in the current configuration. Therefore, the quantities (i.e. displacements, stresses, etc.) on different sides of the interface are denoted using subscripts ‘+’ and ‘-’ in the same way as done for the phase boundary problem.

The problem consists in solving Eq. (1) with corresponding boundary conditions (4), (5) enforced at the external boundary of the body and the interface conditions considered below. The first interface condition is the equality of the tractions, Eq. (16). To shorten the expressions below, the following notation is introduced:

$$\vec{p} = \langle \mathbf{P} \rangle \cdot \vec{N}_*, \quad \vec{v} = \llbracket \vec{u} \rrbracket_*, \quad v = |\vec{v}|. \tag{19}$$

The second interface condition describes the traction-separation relation. Two cases are considered below. The first case is the anisotropic linear traction-separation:

$$\mathbf{K} \cdot \vec{p} = -\vec{v}, \quad \vec{X} \in \Gamma_*, \tag{20}$$

where tensor \mathbf{K} is symmetric and is the compliance of the interface. The second considered case is the non-linear traction-separation:

$$\vec{p} = -\frac{\partial W_1}{\partial \vec{v}}, \quad \vec{X} \in \Gamma_*, \tag{21}$$

where W_1 is the strain energy density of the interface per unit surface in the reference configuration.

2.3.2. Linear traction-separation

Previously, the handling of the fracture problem using the Nitsche’s approach has been considered in [24] for the case of linear elasticity and linear traction-separation. This subsection generalises the results of [24] for the case of large deformations and arbitrary constitutive relations.

First, additional tensor \mathbf{S}_h is introduced:

$$\mathbf{S}_h = \left(\frac{h}{\lambda} \mathbf{I} + \mathbf{K} \right)^{-1}, \tag{22}$$

Then, the energy of the interface (the crack opening) can be written as

$$\begin{aligned} \Pi_*^L &= \int_{\Gamma_*} \left(\frac{1}{2} \mathbf{S}_h : (\llbracket \vec{u} \rrbracket_* + \mathbf{K} \cdot \vec{p}) (\llbracket \vec{u} \rrbracket_* + \mathbf{K} \cdot \vec{p}) - \vec{p} \cdot \llbracket \vec{u} \rrbracket_* - \frac{1}{2} \mathbf{K} : \vec{p} \vec{p} \right) d\Gamma_* = \\ &= \int_{\Gamma_*} \left(\frac{1}{2} \mathbf{S}_h : \llbracket \vec{u} \rrbracket_* \llbracket \vec{u} \rrbracket_* - \frac{h}{\lambda} \mathbf{S}_h : \llbracket \vec{u} \rrbracket_* \vec{p} + \frac{1}{2} \frac{h}{\lambda} \vec{p} \vec{p} : \left(\frac{h}{\lambda} \mathbf{S}_h - \mathbf{I} \right) \right) d\Gamma_*, \end{aligned} \tag{23}$$

where the first line is the direct generalisation of the results of [24] to the case of large deformations (clarification is given at the end of the subsection), while the second line is obtained by the rearrangement of the terms (i.e. \mathbf{K} is expanded into $\mathbf{K} + h\lambda^{-1}\mathbf{I} - h\lambda^{-1}\mathbf{I}$, first two terms of which are replaced by \mathbf{S}_h^{-1} , followed by expansion of the brackets).

The relatively complex form of Eq. (23) results from the requirement to obtain certain particular cases as tensor \mathbf{K} approaches zero or infinity. It can be seen that when \mathbf{K} is zero, the case of a phase boundary is obtained:

$$\Pi_*^L|_{\mathbf{K}=\mathbf{0}} = \Pi_*^B. \tag{24}$$

When \mathbf{K} approaches infinity, the energy becomes proportional to h and disappears as $h \rightarrow 0$, which corresponds to the free surface. Assuming that \mathbf{K}^{-1} exists, it can be written as

$$\Pi_*^L|_{\mathbf{K}^{-1} \rightarrow \mathbf{0}} = - \int_{\Gamma_*} \frac{1}{2} \frac{h}{\lambda} \vec{p} \cdot \vec{p} d\Gamma_*. \tag{25}$$

To get the weak form for this problem, a variation of Π_*^L is performed. Since linear traction-separation is considered, i.e. constant \mathbf{K} , it is useful to denote this variation with $\delta\mathbf{K} = \mathbf{0}$, as non-linear traction-separation is considered later. From the definition of \vec{p} , Eq. (19), it follows that

$$\delta\vec{p} = \vec{N}_* \cdot \left\langle \frac{\partial \mathbf{P}^T}{\partial \mathbf{F}} : \nabla_0 \vec{\varphi} \right\rangle. \tag{26}$$

This can then be used to obtain $\delta\Pi_*^L$ directly from the second line of Eq. (23),

$$\begin{aligned} \delta\Pi_*^L|_{\delta\mathbf{K}=\mathbf{0}} &= \int_{\Gamma_*} \left(\mathbf{S}_h : \left(\llbracket \vec{u} \rrbracket_* - \frac{h}{\lambda} \vec{p} \right) \llbracket \vec{\varphi} \rrbracket_* - \right. \\ &\quad \left. - \frac{h}{\lambda} \left(\left(\llbracket \vec{u} \rrbracket_* - \frac{h}{\lambda} \vec{p} \right) \cdot \mathbf{S}_h + \vec{p} \right) \cdot \vec{N}_* : \left\langle \frac{\partial \mathbf{P}^T}{\partial \mathbf{F}} : \nabla_0 \vec{\varphi} \right\rangle \right) d\Gamma_*, \end{aligned} \tag{27}$$

which results in weak form (12) with the following interfacial term:

$$\text{for crack opening problem with linear traction-separation } \delta\Pi_* = \delta\Pi_*^L|_{\delta\mathbf{K}=\mathbf{0}}.$$

It should be noted that in [24], only the weak form is given, which is derived directly from the strong form, and not from the energy. To see that this paper indeed presents a generalisation of the method of [24] to the case of large deformations, a variation of the first line of Eq. (23) must be taken, which gives:

$$\begin{aligned} \delta\Pi_*^L|_{\delta\mathbf{K}=\mathbf{0}} &= \int_{\Gamma_*} \left(\mathbf{S}_h : \llbracket \vec{u} \rrbracket_* \llbracket \vec{\varphi} \rrbracket_* - (\mathbf{I} - \mathbf{S}_h \cdot \mathbf{K}) : \vec{p} \llbracket \vec{\varphi} \rrbracket_* - (\mathbf{I} - \mathbf{K} \cdot \mathbf{S}_h) : \llbracket \vec{u} \rrbracket_* \delta\vec{p} - \right. \\ &\quad \left. - (\mathbf{K} \cdot (\mathbf{I} - \mathbf{S}_h \cdot \mathbf{K})) : \vec{p} \delta\vec{p} \right) d\Gamma_*. \end{aligned} \tag{28}$$

This expression has exactly the same structure as the corresponding term in Eq. (6) of Ref. [24], apart from the use of the Piola–Kirchhoff tractions instead of the Cauchy tractions and the integration in the reference configuration. In [24], product of \mathbf{S}_h and \mathbf{K} is commutative due to the chosen structure of \mathbf{K} .

2.3.3. Non-linear traction-separation

The non-linear traction-separation is given by Eq. (21). To use the results of Section 2.3.2, it is necessary to define tensor \mathbf{K} for the case of non-linear traction-separation. Thus, assuming that there exists some tensor \mathbf{K} such that condition (20) is fulfilled, it is possible to write the following interface energy:

$$\Pi_*^N = \Pi_*^L + \int_{\Gamma_*} \left(W_1 - \frac{1}{2} \vec{g} \cdot \llbracket \vec{u} \rrbracket_* \right) d\Gamma_*, \tag{29}$$

where

$$\vec{g} = \frac{\partial W_1}{\partial \vec{v}}. \tag{30}$$

Here it can be seen that for an exact solution (with exactly fulfilled interfaces conditions), energy Π_*^N becomes simply an integral of W_1 over surface Γ_* . Term added in Eq. (29) can be viewed as the correction for the non-linear case and when W_1 is quadratic (assuming that K^{-1} exists), the non-linear case becomes the linear case:

$$\Pi_*^N|_{W_1=\vec{v}\cdot K^{-1}\cdot\vec{v}/2} = \Pi_*^L. \tag{31}$$

Although it is possible to consider the general case, where W_1 depends on \vec{v} , in large deformations, it is often assumed that the separation energy depends only on the scalar separation [38], i.e. it is assumed that $W_1 = W_1(v)$. In this case,

$$\vec{g} = \frac{\vec{v}}{v}G, \quad G = \frac{\partial W_1}{\partial v}. \tag{32}$$

The resulting form of \vec{g} , as well as Eqs. (20), (21), (30) leads to the following definition of tensor K for the case of non-linear traction-separation:

$$K \cdot \frac{\vec{v}}{v}G = \vec{v} \quad \Rightarrow \quad K = \frac{v}{G}I = KI, \quad S_h = \frac{1}{K + \frac{h}{\lambda}}I = S_hI, \tag{33}$$

where $K = K(v)$ is a scalar function of v . In the equations below, K' denotes the derivative of K by v .

Before deriving the variation of Π_*^N , it is useful to write the variation of scalar S_h and the derivative of \vec{g} by \vec{v} where K is substituted:

$$\delta S_h = \frac{dS_h}{dv} \delta v = \frac{dS_h}{dv} \frac{\vec{v}}{v} \cdot \delta \vec{v} = -K' S_h^2 \frac{\vec{v}}{v} \cdot \delta \vec{v}, \tag{34}$$

$$\frac{\partial \vec{g}}{\partial \vec{v}} = \frac{1}{K}I + \vec{v} \left(-\frac{K'}{K^2} \right) \frac{\partial v}{\partial \vec{v}} = \frac{1}{K}I - \frac{K'}{vK^2} \vec{v}\vec{v}, \tag{35}$$

Then, using that $\delta W_1 = \vec{g} \cdot \delta \vec{v}$, it is possible to write the variation of the term added in Eq. (29), where Eqs. (32), (33), (35) are used:

$$\delta \Pi_*^N - \delta \Pi_*^L = \int_{\Gamma_*} \left(\frac{1}{2} \vec{g} \cdot \delta \vec{v} - \frac{1}{2} \vec{v} \cdot \delta \vec{g} \right) d\Gamma_* = \int_{\Gamma_*} \frac{1}{2} \frac{K'}{K^2} v \vec{v} \cdot \delta \vec{v} d\Gamma_*. \tag{36}$$

Now, the variation of Π_*^L should be considered, given that in this subsection, K is not constant. It is required since Π_*^L is the first part of Π_*^N . Most of the terms of the variation of Π_*^L are already given in Eq. (27) and it remains to summarise the terms with δS_h . These terms can be written by taking the second line of Eq. (23), substituting the structure of S_h from Eq. (33) and substituting \vec{p} , which is expressed via \vec{g} according to Eqs. (21), (30), which in turn is expressed via K and \vec{v} according to Eqs. (32), (33). This gives

$$\begin{aligned} \delta \Pi_*^L - \delta \Pi_*^L|_{\delta K=0} &= \int_{\Gamma_*} \delta S_h \left(\frac{1}{2} v^2 + \frac{h}{\lambda} \frac{1}{K} v^2 + \frac{1}{2} \frac{h^2}{\lambda^2} \frac{1}{K^2} v^2 \right) d\Gamma_* = \\ &= \int_{\Gamma_*} (-K') \frac{1}{\left(K + \frac{h}{\lambda}\right)^2} v \vec{v} \cdot \delta \vec{v} \frac{1}{2} \left(1 + 2 \frac{h}{\lambda} \frac{1}{K} + \frac{h^2}{\lambda^2} \frac{1}{K^2} \right) d\Gamma_* = - \int_{\Gamma_*} \frac{1}{2} \frac{K'}{K^2} v \vec{v} \cdot \delta \vec{v} d\Gamma_*. \end{aligned} \tag{37}$$

From Eqs. (36) and (37) it is clearly seen that

$$\delta \Pi_*^N = \delta \Pi_*^L|_{\delta K=0}, \tag{38}$$

which might be perhaps a counter-intuitive result that the variation of the linear separation energy exactly coincides with the variation of a more complex non-linear separation energy. This finally results in weak form (12) with the following interfacial term:

$$\text{for general crack opening problem } \delta \Pi_* = \delta \Pi_*^N = \delta \Pi_*^L|_{\delta K=0}.$$

2.4. Contact

2.4.1. Problem formulation

When the fracture problem in large deformations is considered, the separated surfaces may come into contact. Furthermore, the points that come into contact in the current configuration, can have a finite distance between them in the reference configuration. Therefore, a proper contact resolution is required.

Previously, the handling of the contact problem using the Nitsche’s approach has been considered in [32] for the case of linear elasticity and in [33] for the case of large deformations. Typically, methods that deal with the contact mechanics rely on the contact surfaces conforming to the mesh. A recent exception to this are two novel unfitted finite-element methods for contact in linear elasticity setting [39–41], where the contact conditions are enforced on the embedded interfaces. As highlighted above, the aim of the present paper is to obtain an unfitted method (CutFEM); therefore, the major difference between the contact problem considered here and most previous works is that the contact is always between the surfaces that cut through the elements.

In [33], the total energy functional for the case of large deformations is already suggested (Proposition 2.3 of the reference), which enforces the contact conditions in a Nitsche’s manner and from which the weak form is derived by taking the variation. It can be used directly and can be incorporated into CutFEM. However, as highlighted above, the aim of this paper is to present the functionals for the phase boundary, the crack opening and the contact cases in such a way that one can become a particular case of the other. Since the modification of the energy functional of [33], which achieves this, is not straightforward, a somewhat different method is presented below, which generalises the energy functional of [32] for the case of large deformations and arbitrary constitutive relations. Furthermore, traditionally, in the computational contact mechanics, the quantities are projected from one surface onto another and the integration is performed over the latter surface (the so-called master–slave approach). In this paper, however, the aim is to split the contact conditions into integrals over both contact surfaces and to write a symmetric formulation of the numerical method with respect to the choice of the surfaces (also called an unbiased formulation), which is another major difference to [32].

Interface Γ_* in the reference configuration separates into two surfaces γ_+^* and γ_-^* in the current configuration, parts of which come into contact. In the current configuration, a gap between the surfaces is introduced as

$$\rho_+ = \vec{n}_+^* \cdot (\vec{x}_-^c(\vec{x}_+) - \vec{x}_+) \quad \text{or} \quad \rho_- = \vec{n}_-^* \cdot (\vec{x}_+^c(\vec{x}_-) - \vec{x}_-),$$

where \vec{n}_+^* and \vec{n}_-^* are the outer normals to γ_+^* and γ_-^* , respectively, and it is implied that \vec{x}_-^c and \vec{x}_+^c are obtained by the projection of \vec{x}_+ and \vec{x}_- along normals \vec{n}_+^* and \vec{n}_-^* onto γ_-^* and γ_+^* , respectively, hence are the functions of \vec{x}_+ and \vec{x}_- , respectively. At this point, it is useful to introduce the step functions that define the contact patch itself:

$$\chi_{\pm} = \begin{cases} 1, & \text{if } \rho_{\pm} \leq 0, \\ 0, & \text{if } \rho_{\pm} > 0, \end{cases} \quad (39)$$

and introduce the contact tractions as

$$q_{\pm} = q_{\pm}(\vec{x}_{\pm}) = \vec{n}_{\pm}^* \vec{n}_{\pm}^* : \sigma_{\pm}, \quad \vec{n}_{\pm}^* = \vec{n}_{\pm}^*(\vec{x}_{\pm}), \quad \sigma_{\pm} = \sigma_{\pm}(\vec{x}_{\pm}),$$

where each traction is written as a function of a point of a boundary at which it is calculated. This is done to be able to use traction $q_-(\vec{x}_-)$ at point \vec{x}_- of boundary γ_-^* , as well as traction $q_-(\vec{x}_-^c(\vec{x}_+))$ at point \vec{x}_-^c of boundary γ_-^* that is obtained by the projection of point \vec{x}_+ along normal \vec{n}_+^* from γ_+^* onto γ_-^* , and similarly for q_+ . Sign ‘ \leq ’ in (39) is introduced to account for a possible overlap of the surfaces in the numerical solution. Now, it is possible to write the contact conditions in Hertz–Signorini–Moreau form, including the equality of normal tractions:

$$\rho_{\pm} \geq 0, \quad q_{\pm} \leq 0, \quad \rho_{\pm} q_{\pm} = 0, \quad \vec{x}_{\pm} \in \gamma_{\pm}^*, \quad (40)$$

$$q_{\pm}(\vec{x}_{\pm}) = q_{\mp}(\vec{x}_{\mp}^c(\vec{x}_{\pm})), \quad \vec{x}_{\pm} \in \gamma_{\pm}^*. \quad (41)$$

These are the conditions for a perfect contact, i.e. as soon as the gap between the surfaces is non-zero, the traction becomes zero. It is also useful to introduce the form of the contact conditions for the case of adhesion between the surfaces, i.e. when surfaces come into contact, they can imperfectly ‘glue’:

$$\tilde{K}_{\pm} \geq 0, \quad \tilde{K}_{\pm} \Big|_{q_{\pm} < 0} = 0, \quad \tilde{K}_{\pm} q_{\pm} = \rho_{\pm}, \quad \vec{x}_{\pm} \in \gamma_{\pm}^*, \quad (42)$$

where \tilde{K}_\pm is the non-negative compliance of the interface. When the traction is negative, the compliance is zero, which prevents the negative gap between the surfaces. Symbol ‘ \sim ’ is added above K_\pm to distinguish the compliance in the current and in the reference configurations. It is also useful to rewrite this condition in the reference configuration:

$$Q_\pm = \tilde{n}_\pm^* \cdot \mathbf{P}_\pm \cdot \tilde{N}_\pm^*, \tag{43}$$

$$K_\pm \geq 0, \quad K_\pm|_{Q_\pm < 0} = 0, \quad K_\pm Q_\pm = \rho_\pm, \quad \tilde{X}_\pm \in \Gamma_\pm^*. \tag{44}$$

This condition is structurally similar to condition (20).

Now, the problem can be formulated: it consists in solving Eq. (1) with corresponding boundary conditions (4), (5) enforced at the external boundary of the body and interface conditions (40), (41) for the case of contact without adhesion or interface conditions (41), (42) for the case of contact with adhesion.

Given the contact conditions above, when χ_+ takes value 1 at point \vec{x}_+ and its neighbourhood (understood as the neighbourhood on set γ_+^*), points \vec{x}_+^c (\vec{x}_+) and \vec{x}_+ exactly coincide in space and elements $d\gamma_+^*$ and $d\gamma_-^*$ exactly match (therefore, also $\tilde{n}_+^* = -\tilde{n}_-^*$), and similarly for χ_- . This can be used to write the following assumption:

assume that γ_+^* and γ_-^* are such that

$$\int_{\gamma_+^*} \chi_+ f(\vec{x}_+, \vec{x}_+^c(\vec{x}_+), \tilde{n}_+^*(\vec{x}_+)) d\gamma_+^* = \int_{\gamma_-^*} \chi_- f(\vec{x}_+^c(\vec{x}_-), \vec{x}_-, -\tilde{n}_-^*(\vec{x}_-)) d\gamma_-^*, \tag{45}$$

where f is an arbitrary integrable on γ_\pm^* function. In less precise terms, this assumption means that within a contact patch and its neighbourhood, it is assumed that the surfaces are smooth enough for the integration over one surface to be equivalent to the integration over the other surface. This assumption is used in the derivations below to change the integration from one surface to another. Although it might seem to be restrictive, all performed numerical tests confirm that the weak form, which is obtained using this assumption, works fine in practice.

The integral forms of the equations are considered in the presentation below. In the current configuration, the integration is performed over either γ_+^* or γ_-^* , taking the integrand as depending on either \vec{x}_+ or \vec{x}_- , respectively, and also containing quantities that depend on the projected points either \vec{x}_+^c (\vec{x}_+) or \vec{x}_+^c (\vec{x}_-), respectively. When these integrals are pulled back to the reference configuration, even though the integration is performed over Γ_* , the integrand still depends on either \tilde{X}_+ or \tilde{X}_- , respectively, and also contains either \vec{x}_+^c (\vec{x}_+) or \vec{x}_+^c (\vec{x}_-), respectively, where \vec{x}_+ and \vec{x}_- are images of \tilde{X}_+ and \tilde{X}_- , respectively. These cases must obviously be distinguished. Therefore, to denote that the integrand is taken to depend on either \tilde{X}_+ or \tilde{X}_- , surface Γ_* is written as either Γ_+^* or Γ_-^* , respectively.

Since the contact conditions always involve a point on one surface and its projection onto another, integrals over γ_+^* will not contain \vec{x}_- as such and will only contain \vec{x}_+^c . Therefore, for all quantities that depend on \vec{x}_+^c , e.g. $f(\vec{x}_+^c)$, where f is an arbitrary function, superscript ‘c’ can be dropped, and it is implied that \vec{x}_- in this case is the projection of \vec{x}_+ onto γ_-^* . Furthermore, $f(\vec{x}_-)$ is then simply written as f_- . The same omission of superscript ‘c’ is obviously done for integrals over γ_-^* with quantities depending on \vec{x}_+^c . This allows using the notation that is consistent with the previous sections. Such notation is also consistent with the integration in the reference configuration. For example, when integration is performed over Γ_+^* and there are quantities that depend on \tilde{X}_- , it is implied that \tilde{X}_- is the image of point $\vec{x}_- = \vec{x}_+^c$, which is a projection of \vec{x}_+ from γ_+^* onto γ_-^* , while point \vec{x}_+ is itself the image of \tilde{X}_+ , which belongs to Γ_+^* .

Additional aim here is to write a formulation for the case of the contact that contains the case of the phase boundary as a particular case, i.e. the contact can become “perfect gluing” of the surfaces. For this, a projection tensor is introduced:

$$\mathcal{P}_n = \tilde{n}_+^* \tilde{n}_+^{*T} = \tilde{n}_-^* \tilde{n}_-^{*T}, \tag{46}$$

which is used in the derivations below. The fact that \mathcal{P}_n is symmetric is used in the derivations.

2.4.2. Without adhesion

The energy of the interface can be written as

$$\Pi_*^W = \Pi_*^1 + \Pi_*^2, \tag{47}$$

where

$$\begin{aligned} \Pi_*^1 &= - \int_{\Gamma_+^*} \chi_+ \frac{1}{2} \llbracket \vec{x} \rrbracket_* \cdot \mathcal{P}_n \cdot \mathbf{P}_+ \cdot \vec{N}_+^* d\Gamma_+^* + \int_{\Gamma_-^*} \chi_- \frac{1}{2} \llbracket \vec{x} \rrbracket_* \cdot \mathcal{P}_n \cdot \mathbf{P}_- \cdot \vec{N}_-^* d\Gamma_-^* = \\ &= - \int_{\gamma_+^*} \chi_+ \llbracket \vec{x} \rrbracket_* \cdot \mathcal{P}_n \cdot \langle \boldsymbol{\sigma} \rangle \cdot \vec{n}_+^* d\gamma_+^* = \int_{\gamma_-^*} \chi_- \llbracket \vec{x} \rrbracket_* \cdot \mathcal{P}_n \cdot \langle \boldsymbol{\sigma} \rangle \cdot \vec{n}_-^* d\gamma_-^*, \\ \Pi_*^2 &= \int_{\Gamma_+^*} \chi_+ \frac{1}{4} \frac{\beta}{h} \mathcal{P}_n : \llbracket \vec{x} \rrbracket_* \llbracket \vec{x} \rrbracket_* d\Gamma_+^* + \int_{\Gamma_-^*} \chi_- \frac{1}{4} \frac{\beta}{h} \mathcal{P}_n : \llbracket \vec{x} \rrbracket_* \llbracket \vec{x} \rrbracket_* d\Gamma_-^*, \end{aligned} \tag{48}$$

and β is the penalty parameter (similar to λ introduced previously, but it is useful to use a different letter for the contact problem). In Π_*^1 , the transformation between the configurations and equality (45) are used to show that it is possible to write the energy in the reference configuration or in the current configuration with respect to γ_+^* or γ_-^* . It can be seen that in the current configuration, energy Π_*^W almost exactly matches the corresponding term in Eq. (6) of Ref. [32], where the linear elasticity case has been considered. To match the expressions exactly, term Π_*^2 should be written in the current configuration and with respect to only one surface, γ_+^* or γ_-^* . However, in the linear elasticity case, the area transformation is neglected and using equality (45) it is easy to see that indeed the same form as in Ref. [32] is obtained. Projection tensor \mathcal{P}_n is taken either as function of \vec{n}_+^* when it enters integrals over Γ_+^* or as function of \vec{n}_-^* when it enters integrals over Γ_-^* .

This form of energy is advantageous from several points of view. First, in the reference configuration, terms in Π_*^1 and Π_*^2 are symmetric with respect to the choice of the surfaces. Although there is a different sign in front of the term corresponding to Γ_-^* , by convention of this paper, $\llbracket \vec{x} \rrbracket_* = \vec{x}_+ - \vec{x}_-$, therefore, both terms in Π_*^1 have exactly the same structure, including the signs. Second, the phase boundary case is a particular case of the energy given by Eqs. (47), (48). In the phase boundary case, no projection is performed, i.e. the surface evolves from the reference configuration to the current configuration as one surface and γ_+^* should exactly match γ_-^* for the exact solution. Therefore, $\chi_{\pm} = 1$ everywhere and $\llbracket \vec{x} \rrbracket_* = \llbracket \vec{u} \rrbracket_*$, since \vec{x}_+ and \vec{x}_- correspond to the same \vec{X} in the reference configuration in this case. In addition to that, in the phase boundary case, total tractions and displacements are considered; therefore, $\mathcal{P}_n = \mathbf{I}$. This can be summarised as

$$\Pi_*^W \Big|_{\chi_{\pm}=1, \llbracket \vec{x} \rrbracket_* = \llbracket \vec{u} \rrbracket_*, \mathcal{P}_n = \mathbf{I}} = \Pi_*^B. \tag{49}$$

To obtain the weak form, the variation of Π_*^W is performed in several steps. At first, the variation of Π_*^1 is obtained:⁴

$$\begin{aligned} \delta \Pi_*^1 &= - \int_{\Gamma_+^*} \chi_+ \frac{1}{2} \vec{N}_+^* \llbracket \vec{x} \rrbracket_* : \left(\mathcal{P}_n \cdot \frac{\partial \mathbf{P}_+}{\partial \mathbf{F}_+} + {}^4\mathbf{I}^{RT} : \left(\mathbf{P}_+^T \cdot \frac{\partial \mathcal{P}_n}{\partial \mathbf{F}_+} \right) \right) : \nabla_0 \vec{\varphi}_+ d\Gamma_+^* + \\ &+ \int_{\Gamma_-^*} \chi_- \frac{1}{2} \vec{N}_-^* \llbracket \vec{x} \rrbracket_* : \left(\mathcal{P}_n \cdot \frac{\partial \mathbf{P}_-}{\partial \mathbf{F}_-} + {}^4\mathbf{I}^{RT} : \left(\mathbf{P}_-^T \cdot \frac{\partial \mathcal{P}_n}{\partial \mathbf{F}_-} \right) \right) : \nabla_0 \vec{\varphi}_- d\Gamma_-^* + I^1 + I^2, \end{aligned} \tag{50}$$

where last two terms are written separately:

$$\begin{aligned} I^1 + I^2 &= - \int_{\Gamma_+^*} \chi_+ \frac{1}{2} \llbracket \vec{\varphi} \rrbracket_* \cdot \mathcal{P}_n \cdot \mathbf{P}_+ \cdot \vec{N}_+^* d\Gamma_+^* + \int_{\Gamma_-^*} \chi_- \frac{1}{2} \llbracket \vec{\varphi} \rrbracket_* \cdot \mathcal{P}_n \cdot \mathbf{P}_- \cdot \vec{N}_-^* d\Gamma_-^* = \\ &= - \int_{\Gamma_+^*} \chi_+ \vec{\varphi}_+ \cdot \mathcal{P}_n \cdot \mathbf{J}_+ \langle \boldsymbol{\sigma} \rangle \cdot \mathbf{F}_+^{-T} \cdot \vec{N}_+^* d\Gamma_+^* - \int_{\Gamma_-^*} \chi_- \vec{\varphi}_- \cdot \mathcal{P}_n \cdot \mathbf{J}_- \langle \boldsymbol{\sigma} \rangle \cdot \mathbf{F}_-^{-T} \cdot \vec{N}_-^* d\Gamma_-^*, \end{aligned}$$

where $J_{\pm} = \det(\mathbf{F}_{\pm})$. In Eq. (50), the first two terms account for the variation of \mathcal{P}_n and \mathbf{P}_{\pm} . Terms I^1 and I^2 account for the variation of $\llbracket \vec{x} \rrbracket_*$ in both integrals, which becomes $\llbracket \vec{\varphi} \rrbracket_*$. The first line of the expression for $I^1 + I^2$, however, requires evaluating integrals over one surface, e.g. Γ_+^* , when the test function belonging to the other surface, e.g. $\vec{\varphi}_-$, is non-zero. This is inconvenient from the programming point of view and, therefore, the expression is rewritten such that integrals over Γ_+^* contain only $\vec{\varphi}_+$ and similar for Γ_-^* . To do this, the integrals are pulled forward to the current configuration, hence, the Cauchy stress appears, $\llbracket \vec{\varphi} \rrbracket_*$ is expanded, equality (45) is used to transform the integral with $\vec{\varphi}_-$ and γ_+^* to γ_-^* and the integral with $\vec{\varphi}_+$ and γ_-^* to γ_+^* , and all integrals are pulled back to the reference configuration, hence, terms $J_{\pm} \mathbf{F}_{\pm}^{-T}$ appear.

⁴ Fourth-order identity tensor ${}^4\mathbf{I} = \vec{e}_s \vec{e}_k \vec{e}_k \vec{e}_s$ and its right-transpose ${}^4\mathbf{I}^{RT} = \vec{e}_s \vec{e}_k \vec{e}_s \vec{e}_k$ are used in the equations. Property $\mathbf{A} = {}^4\mathbf{I}^{RT} : \mathbf{A}^T$ for arbitrary \mathbf{A} is used.

Then, the variation of Π_*^2 is obtained:

$$\begin{aligned} \delta \Pi_*^2 &= I^3 + I^4 + \int_{\Gamma_+^*} \chi_+ \frac{1}{4} \frac{\beta}{h} \llbracket \bar{x} \rrbracket_* \llbracket \bar{x} \rrbracket_* : \frac{\partial \mathcal{P}_n}{\partial \mathbf{F}_+} : \nabla_0 \bar{\varphi}_+ d\Gamma_+^* + \\ &+ \int_{\Gamma_-^*} \chi_- \frac{1}{4} \frac{\beta}{h} \llbracket \bar{x} \rrbracket_* \llbracket \bar{x} \rrbracket_* : \frac{\partial \mathcal{P}_n}{\partial \mathbf{F}_-} : \nabla_0 \bar{\varphi}_- d\Gamma_-^*, \end{aligned} \tag{51}$$

where the first two terms are written separately:

$$\begin{aligned} I^3 + I^4 &= \int_{\Gamma_+^*} \chi_+ \frac{1}{2} \frac{\beta}{h} \llbracket \bar{x} \rrbracket_* \cdot \mathcal{P}_n \cdot \llbracket \bar{\varphi} \rrbracket_* d\Gamma_+^* + \int_{\Gamma_-^*} \chi_- \frac{1}{2} \frac{\beta}{h} \llbracket \bar{x} \rrbracket_* \cdot \mathcal{P}_n \cdot \llbracket \bar{\varphi} \rrbracket_* d\Gamma_-^* = \\ &= \int_{\Gamma_+^*} \chi_+ \frac{1}{2} \left(1 + \frac{\eta_-}{\eta_+} \right) \frac{\beta}{h} \llbracket \bar{x} \rrbracket_* \cdot \mathcal{P}_n \cdot \bar{\varphi}_+ d\Gamma_+^* - \int_{\Gamma_-^*} \chi_- \frac{1}{2} \left(1 + \frac{\eta_+}{\eta_-} \right) \frac{\beta}{h} \llbracket \bar{x} \rrbracket_* \cdot \mathcal{P}_n \cdot \bar{\varphi}_- d\Gamma_-^*. \end{aligned}$$

Here again, the variation of \mathcal{P}_n is accounted first and the variation of $\llbracket \bar{x} \rrbracket_*$ in both integrals is written separately. The latter is then transformed in a similar way as above, such that integrals over Γ_+^* contain only $\bar{\varphi}_+$ and similar for Γ_-^* . However, since terms $J_{\pm} \mathbf{F}_{\pm}^{\pm T} \cdot \bar{N}_{\pm}^*$ are not present in the integrals, the area transformation is done differently, as shown below. This gives weak form (12) with the following interfacial term:

$$\text{for contact problem without adhesion } \delta \Pi_* = \delta \Pi_*^W = \delta \Pi_*^1 + \delta \Pi_*^2.$$

For elementary surface elements $d\Gamma$ and $d\gamma$ in the reference and the current configurations, respectively, the following is true:

$$\begin{aligned} J \mathbf{F}^{-T} \cdot \bar{N} d\Gamma &= \bar{n} d\gamma, \\ \bar{N} d\Gamma &= J^{-1} \mathbf{F}^T \cdot \bar{n} d\gamma, \\ (d\Gamma)^2 &= J^{-2} \bar{n} \cdot \mathbf{F} \cdot \mathbf{F}^T \cdot \bar{n} (d\gamma)^2, \\ d\Gamma &= J^{-1} \sqrt{\mathbf{B}} : \bar{n} \bar{n} d\gamma, \end{aligned}$$

where $\mathbf{B} = \mathbf{F} \cdot \mathbf{F}^T$ is the Finger tensor. This can be used in the setting of this paper in the following way:

$$\begin{aligned} \int_{\Gamma_+^*} \chi_+ f d\Gamma_+^* &= \int_{\gamma_+^*} \chi_+ f \frac{\sqrt{\mathbf{B}_+ : \bar{n}_+^* \bar{n}_+^*}}{J_+} d\gamma_+^* = \int_{\gamma_-^*} \chi_- f \frac{\sqrt{\mathbf{B}_+ : \bar{n}_+^* \bar{n}_+^*}}{J_+} d\gamma_-^* = \\ &= \int_{\Gamma_-^*} \chi_- f \frac{J_- \sqrt{\mathbf{B}_+ : \bar{n}_+^* \bar{n}_+^*}}{J_+ \sqrt{\mathbf{B}_- : \bar{n}_-^* \bar{n}_-^*}} d\Gamma_-^* = \int_{\Gamma_-^*} \chi_- f \frac{\eta_+}{\eta_-} d\Gamma_-^*, \end{aligned} \tag{52}$$

where equality (45) is used and notation η_{\pm} is introduced.

Finally, the derivative of \mathcal{P}_n by \mathbf{F}_{\pm} must be written. Since \mathcal{P}_n is always taken as function of either \bar{n}_+^* or \bar{n}_-^* according to Eq. (46), the subscripts are omitted below:

$$\begin{aligned} \bar{n}^* \bar{n}^* &= \frac{\bar{c} \bar{c}}{|\bar{c}|^2}, \quad \bar{c} = \mathbf{F}^{-T} \cdot \bar{N}^*, \\ \frac{\partial (\bar{n}^* \bar{n}^*)}{\partial \mathbf{F}} &= -2 \frac{\bar{c} \bar{c}}{|\bar{c}|^4} \bar{c} \cdot \frac{\partial \bar{c}}{\partial \mathbf{F}} + \frac{1}{|\bar{c}|^2} (4\mathbf{I} + 4\mathbf{I}^{RT}) : \bar{c} \frac{\partial \bar{c}}{\partial \mathbf{F}}, \quad \frac{\partial \bar{c}}{\partial \mathbf{F}} = \bar{N}^* \cdot \frac{\partial \mathbf{F}^{-1}}{\partial \mathbf{F}}. \end{aligned}$$

2.4.3. With adhesion

Before the interfacial energy is outlined, additional quantities similar to Eq. (33) are introduced:

$$S_{\pm}^h = \frac{1}{K_{\pm} + \frac{h}{\beta}}, \quad \zeta_{\pm} = \frac{1}{2} \frac{h}{\beta} \left(\frac{h}{\beta} S_{\pm}^h - 1 \right), \quad \chi_{\pm}^a = \frac{h}{\beta} S_{\pm}^h. \tag{53}$$

For now, K_{\pm} is taken to be a constant. Next, the interfacial energy of the contact with adhesion is written similar to Eq. (23) in the following way:

$$\begin{aligned} \Pi_*^A &= \Pi_*^W|_{\chi_{\pm}=\chi_{\pm}^a} + \int_{\Gamma_*^+} \frac{\zeta_+}{2} \vec{N}_+^* \cdot \mathbf{P}_+^T \cdot \mathcal{P}_n \cdot \mathbf{P}_+ \cdot \vec{N}_+^* d\Gamma_*^+ + \\ &+ \int_{\Gamma_*^-} \frac{\zeta_-}{2} \vec{N}_-^* \cdot \mathbf{P}_-^T \cdot \mathcal{P}_n \cdot \mathbf{P}_- \cdot \vec{N}_-^* d\Gamma_*^-. \end{aligned} \tag{54}$$

The new terms introduced in Eq. (54) are symmetric with respect to the choice of the surfaces.

Energy (54) can be viewed as a modified version of energy (23) for the case of contact with adhesion, although it is not strictly a generalisation of it. In the crack opening case, no projection is performed, surface Γ_* in the reference configuration splits into two surfaces in the current configuration; however, the opening in the current configuration is calculated between the points that coincide in the reference configuration, therefore, $[[\vec{x}]]_* = [[\vec{u}]]_*$. In Eq. (54), term Π_*^W taken at $\chi_{\pm} = \chi_{\pm}^a$ corresponds to the first two terms of the second line of Eq. (23), and when $[[\vec{x}]]_* = [[\vec{u}]]_*$ and $\mathcal{P}_n = \mathbf{I}$, it is easy to see that these parts match exactly. The last two terms introduced in energy (54) correspond to the last term of the second line of Eq. (23); however, they are not equal and to obtain the exact match, it is necessary to use interface condition (16). This can be summarised as:

$$\Pi_*^A|_{[[\vec{x}]]_*=[[u]]_*, \mathcal{P}_n=\mathbf{I}, \mathbf{P}_- \cdot \vec{N}_-^* = \mathbf{P}_+ \cdot \vec{N}_+^*, K_+ = K_-} = \Pi_*^L|_{K=KI} \tag{55}$$

The variation of the energy is performed:

$$\delta \Pi_*^A = \delta \Pi_*^W|_{\chi_{\pm}=\chi_{\pm}^a} + I_+^A + I_-^A, \tag{56}$$

where

$$I_{\pm}^A = \int_{\Gamma_{\pm}^*} \frac{\zeta_{\pm}}{2} \vec{N}_{\pm}^* \cdot \left(\mathbf{P}_{\pm}^T (\mathbf{P}_{\pm} \cdot \vec{N}_{\pm}^*) : \frac{\partial \mathcal{P}_n}{\partial \mathbf{F}_{\pm}} + 2 \mathbf{P}_{\pm}^T \cdot \mathcal{P}_n \vec{N}_{\pm}^* : \frac{\partial \mathbf{P}_{\pm}^T}{\partial \mathbf{F}_{\pm}} \right) : \nabla_0 \vec{\varphi}_{\pm} d\Gamma_{\pm}^*. \tag{57}$$

Variation $\delta \Pi_*^W$ in (56), however, must be taken carefully, as equality (45) does not hold for the contact with adhesion, since the surfaces can be at a finite distance and the integration over one surface cannot be directly replaced by the integration over the other surface. Equality (45) was used in two places in the derivation of $\delta \Pi_*^W$ — in $I_1 + I_2$ and in $I_3 + I_4$ to go from the first line to the second line of the corresponding expressions. This means that in the general case (an exception is discussed below), first lines of the expressions for $I_1 + I_2$ and $I_3 + I_4$ must be used when substituted to (56). This finally gives weak form (12) with the following interfacial term:

for contact problem with adhesion $\delta \Pi_* = \delta \Pi_*^A$.

So far, K_{\pm} has been taken to be a constant, which of course does not prevent the volumes to overlap, i.e. it does not prevent a negative gap between the surfaces, as it does not enforce contact conditions (44). Therefore, K_{\pm} must be a function of Q_{\pm} and ρ_{\pm} , and, in addition to this, a non-linear energy density must be added, as done during the transition from Eq. (23) to Eq. (29). In the crack opening case, it has been shown that the addition of such term and the consideration of a non-linear compliance does not change the weak form, as shown in Eq. (38). It can be easily seen⁵ that Π_*^A has the same structure as Π_*^L . Therefore, the derivation analogous to Eqs. (36) and (37) will show that the addition of analogous to (29) energy term and the consideration of $K_{\pm}(Q_{\pm}, \rho_{\pm})$ will result in the same form with $\delta \Pi_* = \delta \Pi_*^A$ derived above.

One practical purpose of the case of contact with adhesion is the introduction of the ‘numerical’ adhesion to accelerate and stabilise the convergence when the Newton–Raphson method is used to solve the system of equations. For example, the compliance can be taken as

$$K_{\pm} = \begin{cases} 0, & \text{if } Q_{\pm} < 0, \\ A \left| \frac{\rho_{\pm}}{h} \right|^s, & \text{if } Q_{\pm} \geq 0, \end{cases} \tag{58}$$

⁵ Energy Π_*^A can be rewritten with $Q_{\pm}, \rho_{\pm}, \chi_{\pm}^a, \zeta_{\pm}, \mathcal{P}_n$ substituted into it:

$$\Pi_*^A = \Pi_*^{A+} + \Pi_*^{A-}, \quad \Pi_*^{A\pm} = \int_{\Gamma_{\pm}^*} \left(\frac{1}{4} S_{\pm}^h \rho_{\pm}^2 + \frac{1}{2} \frac{h}{\beta} S_{\pm}^h \rho_{\pm} Q_{\pm} + \frac{1}{4} \frac{h}{\beta} \left(\frac{h}{\beta} S_{\pm}^h - 1 \right) Q_{\pm}^2 \right) d\Gamma_{\pm}^*,$$

which has the same structure as Π_*^L , only split into two integrals, each taken with 1/2. Different sign in front of the second term is due to the definition of ρ_{\pm} . For derivation analogous to (37), condition $K_{\pm} Q_{\pm} = \rho_{\pm}$ from (44) must be used.

where A and $s > 1$ are constants, and when $h \rightarrow 0$ it can be seen that the ideal contact is obtained — zero compliance if traction is negative, infinite compliance (free boundary) otherwise.

For such numerical adhesion, assumption (45) can be used. Surfaces γ_{\pm}^* can be separated into parts that are in the perfect contact ($Q_{\pm} < 0$) and parts that are distanced ($Q_{\pm} \geq 0$). Assumption (45) can be used for the former in the same way it was used in Section 2.4.2. When assumption (45) is used for the latter, a shift is introduced in the energy; however, since the adhesion is numerical, the energy density for these parts goes to zero when $h \rightarrow 0$ anyway. Therefore, any form of terms $I_1 + I_2$ and $I_3 + I_4$ in $\delta\Pi_*^W$ can be used when substituted into $\delta\Pi_*^A$, including the convenient from the programming point of view form with integrals over Γ_+^* and Γ_-^* containing only $\bar{\varphi}_+$ and $\bar{\varphi}_-$, respectively.

2.5. Stabilisation term

As mentioned above, the outline of the finite-element formulation of the method, given the weak form, is relatively standard and can be found in Appendix. Since the interface can partition some elements into highly unequal area fractions, additional numerical stabilisation terms are introduced in CutFEM, e.g. [1,29], to avoid ill-conditionality of the system of equations.

In the finite-element formulation, the set of all elements is denoted as \mathcal{T} , the sets of elements that cover Ω_+ and Ω_- are denoted as \mathcal{T}_+ and \mathcal{T}_- , respectively, and the set of elements that are intersected by the interface is denoted as $\mathcal{T}_* = \mathcal{T}_+ \cap \mathcal{T}_-$. The set of all element boundaries is denoted as \mathcal{F} . The set of boundaries of all elements that are intersected by the interface is denoted as

$$\mathcal{F}_* = \{F \mid F \in \mathcal{F}, E \in \mathcal{T}_*, F \cap E \neq \emptyset\}.$$

Next, it is necessary to define the sets of element boundaries that have two adjacent elements from the same element set (\mathcal{T}_+ or \mathcal{T}_-):

$$\mathcal{F}_{\pm}^* = \{F \mid F \in \mathcal{F}_*, \exists E_1 \in \mathcal{T}_{\pm}, \exists E_2 \in \mathcal{T}_{\pm}, F \cap E_1 \neq \emptyset, F \cap E_2 \neq \emptyset\}.$$

The stabilisation term is added as an additional term Π_I to the energy:

$$\Pi_I = \sum_{\Gamma_f \in \mathcal{F}_+^*} \frac{\kappa h}{2} \int_{\Gamma_f} \llbracket \mathbf{F}_+ \cdot \vec{N}_f \rrbracket_e^2 d\Gamma_f + \sum_{\Gamma_f \in \mathcal{F}_-^*} \frac{\kappa h}{2} \int_{\Gamma_f} \llbracket \mathbf{F}_- \cdot \vec{N}_f \rrbracket_e^2 d\Gamma_f, \tag{59}$$

where \vec{N}_f is the normal to boundary Γ_f , κ is the stabilisation parameter and $\llbracket \cdot \rrbracket_e$ denotes the jump of the quantity across the element boundary. The orientation of normal \vec{N}_f is not important, as the jump is squared. The variation of the stabilisation term leads to

$$\begin{aligned} \delta\Pi_I &= \sum_{\Gamma_f \in \mathcal{F}_+^*} \kappa h \int_{\Gamma_f} \llbracket \mathbf{F}_+ \cdot \vec{N}_f \rrbracket_e \cdot \llbracket (\nabla_0 \bar{\varphi}_+)^T \cdot \vec{N}_f \rrbracket_e d\Gamma_f + \\ &+ \sum_{\Gamma_f \in \mathcal{F}_-^*} \kappa h \int_{\Gamma_f} \llbracket \mathbf{F}_- \cdot \vec{N}_f \rrbracket_e \cdot \llbracket (\nabla_0 \bar{\varphi}_-)^T \cdot \vec{N}_f \rrbracket_e d\Gamma_f. \end{aligned} \tag{60}$$

3. Computational examples

3.1. Geometry, constitutive laws and parameters

The proposed method has been implemented in MATLAB. For all computational examples, the geometry in the reference configuration is the unit square. The structured mesh consisting of linear finite elements is used. The elements of the mesh are isosceles right triangles with side lengths of h . The plane strain problem formulation is considered. Therefore, the matrix notation of the total deformation gradient tensor is given by

$$\underline{F} = \begin{pmatrix} \frac{\partial x_1}{\partial X_1} & \frac{\partial x_1}{\partial X_2} & 0 \\ \frac{\partial x_2}{\partial X_1} & \frac{\partial x_2}{\partial X_2} & 0 \\ 0 & 0 & 1 \end{pmatrix}.$$

Thus, unknown displacements \vec{u} are vectors in the 12-plane.

The hyperelastic constitutive behaviour is assumed for both phases [42,43]:

$$W_{\pm} = k (J_{\pm} - 1 - \ln J_{\pm}) + \frac{\mu}{2} (\text{tr}(\bar{\mathbf{B}}_{\pm}) - 3), \quad \mathbf{P}_{\pm} = \frac{\partial W_{\pm}}{\partial \mathbf{F}_{\pm}}, \quad (61)$$

where

$$\bar{\mathbf{B}}_{\pm} = (J_{\pm})^{-\frac{2}{3}} \mathbf{F}_{\pm} \cdot \mathbf{F}_{\pm}^T, \quad J_{\pm} = \det(\mathbf{F}_{\pm}). \quad (62)$$

Closed-form expressions for the first and the second derivatives of W_{\pm} with respect to \mathbf{F}_{\pm} can be found in the appendix of Ref. [31].

For crack opening, the following non-linear energy density of the interface is used:

$$W_I = \psi \left(1 - \left(1 + \frac{v}{a} \right) \exp\left(-\frac{v}{a}\right) \right), \quad (63)$$

where ψ and a are the interaction parameters. Scalar traction G at the interface, defined in Eq. (32), reaches maximum at $v = a$ and decays approximately exponentially at $v > a$.

Since the purpose of this paper is the presentation of a numerical method, units are omitted for the parameter values. For the examples below, bulk modulus $k = 10$ and shear modulus $\mu = 2$ were taken. Interface separation parameters ψ and a , the numerical parameters $(h, \lambda, \beta, \kappa)$ and the boundary conditions are varied for different examples and the values are given below. In the Newton–Raphson method, absolute tolerances for the ℓ^{∞} -norms of the function and of the change of the solution were taken to be 10^{-11} .

3.2. Flat interface and homogeneous deformation

First, it is necessary to ensure that for the case of homogeneous deformation, the proposed method exactly recovers the solution, up to the machine accuracy, i.e. it does not introduce any surplus errors. This idea can be understood along the lines of the so-called patch test in the finite-element methods, where the boundary conditions corresponding to the homogeneous solution (i.e. constant deformation gradient) are applied, and the numerically obtained solution should match the analytical solution up to the machine accuracy. The testing is performed in three steps: the crack opening for the general case of the non-linear traction separation (Section 3.2.1), the contact without adhesion (Section 3.2.2) and the contact with adhesion (Section 3.2.3). For these subsections, a flat interface $X_2 = 11/19$ is created and uniaxial loading boundary conditions are used:

$$\begin{aligned} u_2|_{X_2=0} &= 0, & u_1|_{X_1=0, X_2=0} &= 0, \\ u_2|_{X_2=1} &= u^0, & u_1|_{X_1=0, X_2=1} &= 0. \end{aligned}$$

Since this section deals with the flat interface and homogeneous deformation, it is sufficient to report the results in text, without showing the plots.

3.2.1. Crack opening

The crack opening case tests specifically weak form (12) with $\delta \Pi_*^N$. For this example, physical parameters $\psi = 0.0049$, $a = 0.07$ and numerical parameters $h = 1/16$, $\lambda = 10^4$, $\kappa = 10^{-3}$ are used. Two different loading scenarios (both uniaxial tension) are considered: $u^0 = 0.05$ and $u^0 = 0.1$. Even though the problem is non-linear, since the deformation is homogeneous, it is easy to obtain the analytical solution. When the analytical solution was compared to the numerical solution, the difference between the displacements was order of 10^{-16} , which is the order of the default machine precision of MATLAB. This means that the proposed method and the implementation for the crack opening case with non-linear traction separation passes the test case of homogeneous deformation.

3.2.2. Contact, compression

Next, it is necessary to test weak form (12) with $\delta \Pi_*^W$, which is the case of contact. The case of uniaxial compression with $u^0 = -0.01$ is considered. Numerical parameters $h = 1/16$, $\kappa = 10^{-3}$ are used and $\beta \in \{1, 10, 100\}$ is considered. The relevant quantity in the case of contact is the distance between the surfaces. In the numerical solution, the negative gap was order of 10^{-16} , again the order of the machine precision. This coincides with the other versions of the contact conditions imposed using the Nitsche's method — in [32], the considered example “elastic block on elastic block” also resulted in a gap order of 10^{-16} . Due to boundary conditions, only

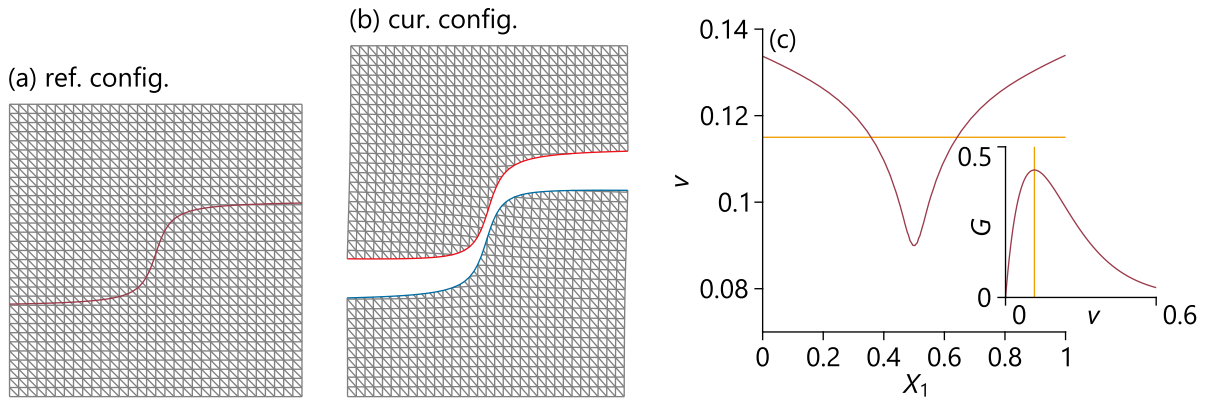


Fig. 1. The geometry of the body in the reference configuration (a) and in the current configuration (b). The interfacial gap (c) as a function of X_1 coordinate of the interfacial point in the reference configuration and the traction-separation law used in the simulations. The horizontal line indicates the gap equal to a . The calculations shown in the plots were performed for $h = 1/32$, $\lambda = 10^4$, $\kappa = 10^{-2}$.

22 and 33 components of the first Piola–Kirchhoff stress are expected to be non-zero and the numerical solution resulted in $P_{22} = -0.0683$ and $P_{33} = -0.0277$. The spread of the values of the components of the first Piola–Kirchhoff stress across all elements, i.e. $(\max P_{ij} - \min P_{ij})$ over all elements for ij component of \mathbf{P} , was order of 10^{-13} – 10^{-14} .

3.2.3. Contact with adhesion, tension

Finally, it is necessary to verify that the adhesion works correctly in the case of contact, i.e. weak form (12) with $\delta \Pi_*^A$. For this example, physical compliance of the adhesion is imposed

$$K_{\pm} = \frac{a^2}{\psi} \exp\left(\frac{\rho_{\pm}}{a}\right),$$

with parameters $\psi = 0.0049$, $a = 0.07$. Two different tensile loadings are considered: $u^0 = 0.05$ and $u^0 = 0.1$. Such setup corresponds to the same analytical solution as in Section 3.2.1. Numerical parameters $h = 1/16$, $\beta = 10^3$, $\kappa = 10^{-3}$ are used. Again, when the solutions were compared, the difference between the displacements was order of 10^{-16} . This completes the verification for the case of homogeneous deformation.

3.3. Non-homogeneous deformation and convergence rates

3.3.1. Curved interface, crack opening

The next step in testing of the proposed method and its implementation is to verify that the theoretical convergence rate of the finite-element method is approached with decrease of the mesh size. First, the crack opening case is considered, weak form (12) with $\delta \Pi_*^N$. A non-flat interface is given by curve

$$X_2 = \frac{23}{47} + \frac{4}{11\pi} \arctan\left(\frac{33\pi}{4} \left(X_1 - \frac{1}{2}\right)\right),$$

which is shown in Fig. 1a. Uniaxial loading boundary conditions are used:

$$u_2|_{X_2=0} = 0, \quad u_1|_{X_1=0, X_2=0} = 0, \tag{64}$$

$$u_2|_{X_2=1} = u^0, \tag{65}$$

with $u^0 = 0.2$. Physical parameters $\psi = 0.1323$, $a = 0.115$ and numerical parameters $h = 1/N$, $N \in \{2^2, 2^3, \dots, 2^9\}$, $\lambda \in \{10^3, 10^4, 10^5\}$, $\kappa \in \{10^{-2}, 10^{-1}, \dots, 10^2\}$ are used.

The deformed state of the geometry is shown in Fig. 1b. It can be seen that due to the curvature of the interface, the traction varies along the interface, which leads to slight rotation of the regions to the left and to the right of the central part of the interface. The interfacial gap as a function of X_1 is shown in Fig. 1c, with the traction-separation

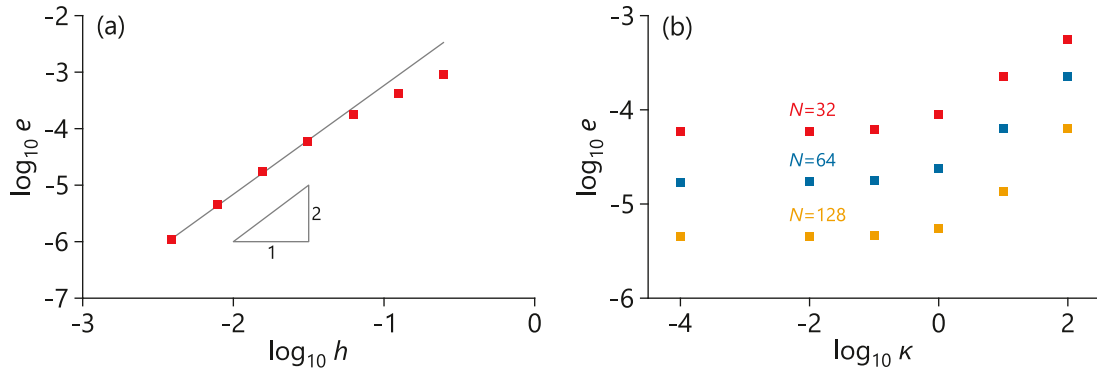


Fig. 2. The dependence of the error on the mesh size (a) and on the inter-element stabilisation parameter (b). The error was calculated as the ℓ^2 -norm of the difference between the current solution and the reference solution with mesh size $h = 1/840$. Parameter $\lambda = 10^4$ was used in the calculations. The calculations in (a) were performed for $\kappa = 10^{-2}$.

law shown in the inset of the figure. Value $v = a$, which corresponds to the maximum traction, is indicated by the horizontal line on both figures. It can be seen that in the considered problem, the traction-separation relation is in the highly non-linear regime.

To analyse the convergence, the reference solution with mesh size $h = 1/840$ was calculated. The solutions with different mesh sizes were compared at the nodes of the mesh with $h_c = 1/4$, i.e. $M = 25$ comparison points were selected. The error was calculated as the ℓ^2 -norm of the difference between the solutions taken at the comparison points:

$$e(h_1, h_2) = \frac{1}{M} \|U^{h_1} - U^{h_2}\|_{\ell^2}, \tag{66}$$

where U^{h_1} and U^{h_2} are solutions with mesh sizes h_1 and h_2 , respectively, taken at the comparison points.⁶ The convergence is shown in Fig. 2a and the calculated rate (i.e. the slope of the linear fit) is $r = 1.93$, which is close to the theoretical quadratic convergence for linear elements. Furthermore, the influence of numerical parameter κ on the numerical error was investigated and is shown in Fig. 2b. The introduction of the stabilisation term somewhat increases the error; however, it can be seen that for small κ this increase is negligible, while such stabilisation term can be important for cases when the interface cuts a small area fraction in some elements.

The convergence rate was also evaluated pointwise:

$$r = r(\vec{X}, h) = \log_2 \frac{|\vec{u}^h(\vec{X}) - \vec{u}^{h/2}(\vec{X})|}{|\vec{u}^{h/2}(\vec{X}) - \vec{u}^{h/4}(\vec{X})|}, \tag{67}$$

where r is the convergence rate at point \vec{X} and \vec{u}^h is the numerical solution obtained with mesh size $h = 1/N$. The pointwise convergence rate at three lines across the computational domain, $X_2 = 1/4$, $X_2 = 1/2$, $X_2 = 3/4$, is shown in Fig. 3 as a function of X_1 . In Figs. 3a–c, the mesh size is varied and it can be seen that with the decrease of h , the convergence rate approaches the expected value of 2, which is the theoretical convergence rate for linear finite elements.

In Figs. 3d–f, parameter κ is varied and it can be seen that up to $\kappa = 10^1$, the convergence rate is still around the theoretical convergence rate of 2; however, for $\kappa = 10^2$, the rate drops due to overconstrained inter-element jump of the deformation gradient in the intersected elements and such values of κ should be avoided. This coincides with the results for the previously-proposed method for handling the phase boundaries using the cut-element technique [31].

⁶ Column U^h can be formally defined as

$$U_{2N_c i + 2j + k}^h = \vec{e}_k \cdot \vec{u}^h(\vec{X}_{ij}), \quad \vec{X}_{ij} = \vec{e}_1 h_c i + \vec{e}_2 h_c j, \quad i, j \in \{0, 1, \dots, N_c\}, \quad k \in \{1, 2\},$$

where \vec{u}^h is the numerical solution obtained with mesh with size h , while $h_c = 1/N_c$ is the size of the coarse mesh, nodes of which are taken as the comparison points.

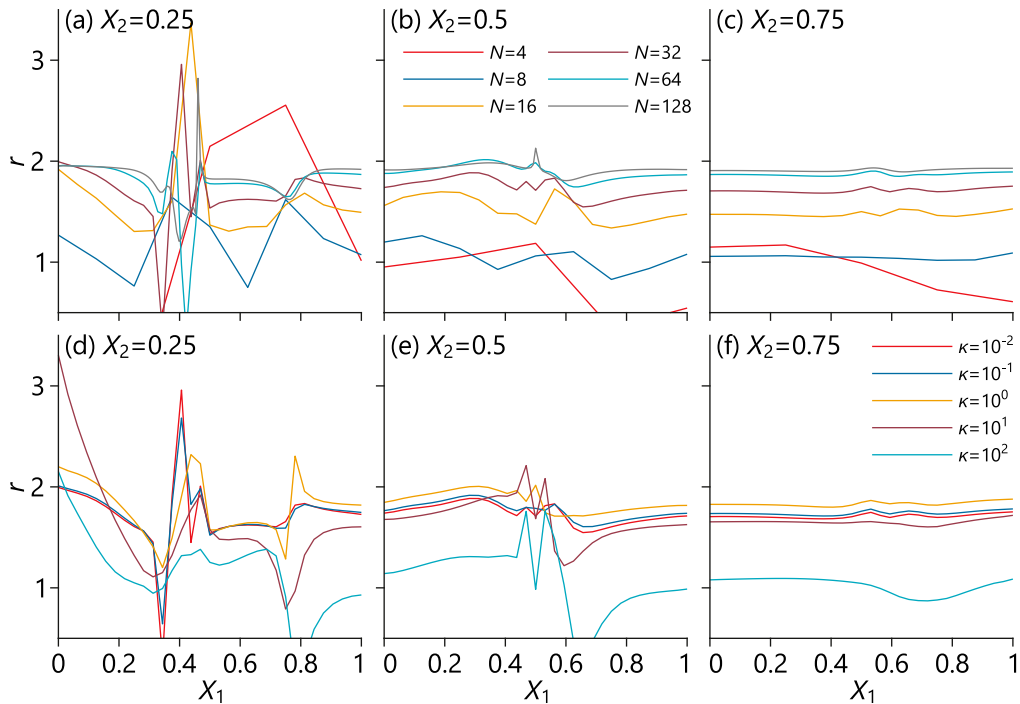


Fig. 3. The pointwise convergence rate on lines $X_2 = 1/4$ (a,d), $X_2 = 1/2$ (b,e) and $X_2 = 3/4$ (c,f) as a function of X_1 . Parameters $h = 1/N$ (a,b,c) and κ (d,e,f) are varied. In (a,b,c), the calculations were performed for $\lambda = 10^4$, $\kappa = 10^{-2}$. In (d,e,f), the calculations were performed for $h = 1/32$, $\lambda = 10^4$.

The variation of parameter λ (results are not shown in the figures) showed that for large λ , more specifically $\lambda \in \{10^3, 10^4, 10^5\}$, its influence on the convergence rate is negligible.

3.3.2. Inclined interface, contact, compression

Finally, it is necessary to ensure that the contact conditions do not affect the convergence rate and do not create any surplus tractions. Weak form (12) with $\delta \Pi_*^W$ is considered. Since the convergence rate in the bulk has already been tested in Section 3.3.1, it is only necessary to verify that the behaviour of the interface is correct. This can be done by comparing the total traction on one surface with the total traction on the other surface. In the numerical solution, the difference between these tractions should behave similarly to the error in the stresses, which is $O(h)$ for linear finite elements.

Numerical parameters $h = 1/N$, $N \in \{2^2, 2^3, \dots, 2^7\}$, $\beta \in \{10^{-2}, 10^{-1}, \dots, 10^3\}$, $\kappa = 10^{-3}$ are used. An inclined interface $X_2 = (13 - 6X_1)/23$ is created and the following boundary conditions are used:

$$\vec{u}|_{X_2=0} = \vec{0}, \quad \vec{u}|_{X_2=1} = \vec{u}^0, \tag{68}$$

with $\vec{u}^0 = 0.01(\vec{e}_1 - \vec{e}_2)$. These boundary conditions lead to the slip between the interface surfaces and the contact points fall within various positions within the interface segments, similar to the “non-matching discretisation and non-uniform displacement” example in [32]. The deformed state of the geometry is shown in Fig. 4a. The deformation of the geometry can be seen in the lower and the upper blocks deflecting slightly to the left and to the right, respectively.

The absolute value of the jump of the total tractions acting on the contact surfaces is defined as

$$j = \left| \int_{\Gamma_+^*} \mathbf{P}_+ \cdot \vec{N}_+ d\Gamma_+^* - \int_{\Gamma_-^*} \mathbf{P}_- \cdot \vec{N}_- d\Gamma_-^* \right|, \tag{69}$$

where it can be seen that in j , the first term contains only stresses in the ‘+’ subdomain, while the second term contains only stresses in ‘-’ subdomain. In Fig. 4b, j as a function of the mesh size is shown and it can be seen

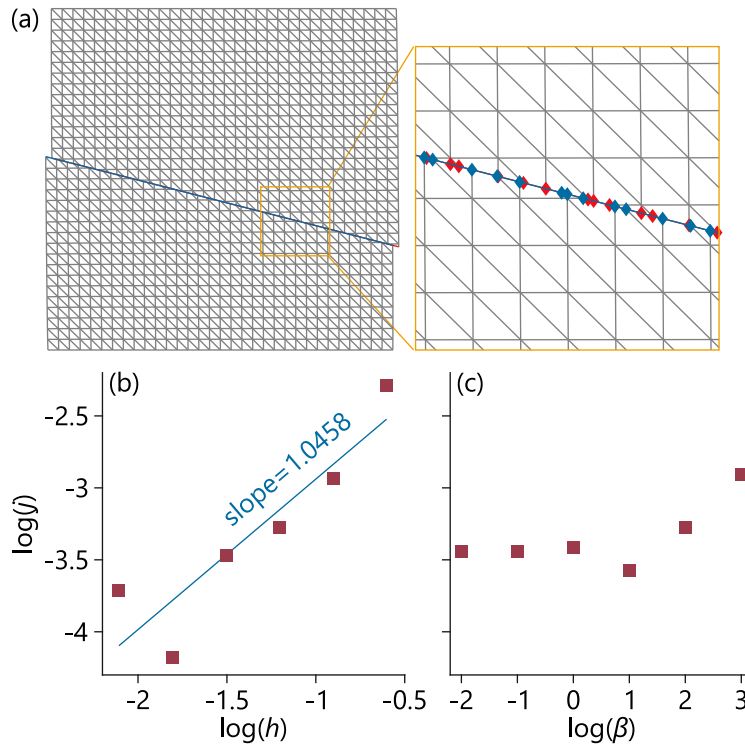


Fig. 4. The geometry of the body in the current configuration (a). The red and the blue diamonds indicate the intersections of the element edges with surfaces γ^* (belonging to the upper subdomain) and γ_+^* (belonging to the lower subdomain), respectively. The absolute value of the jump of the total tractions acting on the contact surfaces as a function of the mesh size (b) and parameter β (c). In (a), the calculation was performed for $h = 1/32$, $\beta = 10^2$; in (b), for $\beta = 10^2$; in (c), for $h = 1/16$.

that, although there is some spread between the points, on average, it converges to zero with the approximate rate of 1, i.e. it behaves as the theoretical error in the stresses. In Fig. 4c, it can be seen that there is no significant influence of the value of β on j .

3.4. Demonstrative examples

So far, the crack opening, the contact without and with adhesion were considered separately in relatively simple scenarios. It is useful to demonstrate the proposed method in more complex conditions, combining together the crack opening with the non-linear traction-separation and the contact with adhesion, by considering weak form (12) with the following interfacial term:

$$\text{for combined crack opening and contact problem } \delta \Pi_* = \delta \Pi_*^N + \delta \Pi_*^A.$$

In this section, three different geometries and corresponding loading cases are considered. Numerical adhesion given by Eq. (58) is used with parameters $A = 10^2$, $s = 1.5$. Numerical parameters $h = 1/32$, $\kappa = 10^{-3}$, $\lambda = 10^4$, $\beta = 10^2$ are used.

3.4.1. Inclusion

The first considered problem is an inclusion inside a matrix. The circular interface is given by curve $(X_1 - 1/2)^2 + (X_2 - 1/2)^2 = 1/5$. Physical parameters of the interface $\psi = 1$, $a = 1$ are taken. Uniaxial loading boundary conditions (64), (65) are used with u^0 varied from 0 to 0.3. The deformed configuration at $u^0 \in \{0.1, 0.2, 0.3\}$ is shown in Fig. 5. The matrix material stretches and debonds from the inclusion at the upper and the lower parts of the inclusion. At the left and at the right sides of the inclusion, the matrix frictionlessly slides around the inclusion and subjects inclusion to compressive stresses, which can be seen from the deformed mesh of

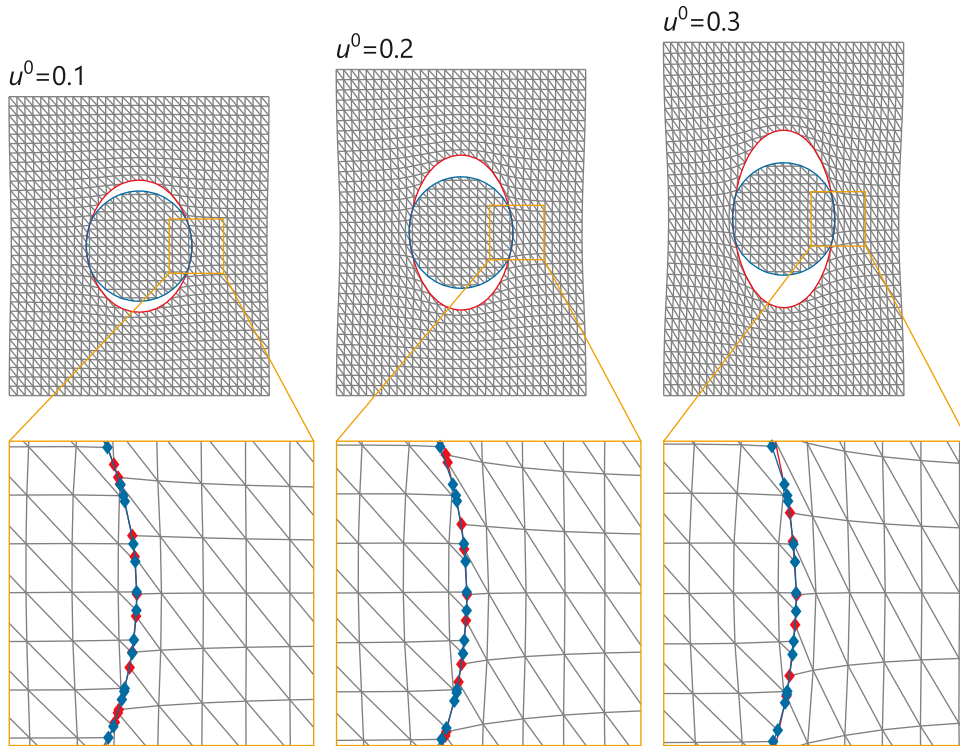


Fig. 5. The geometry of the body in the current configuration for the case of the inclusion inside the matrix. The red and the blue diamonds indicate the intersections of the element edges with surfaces γ_-^* (belonging to the matrix) and γ_+^* (belonging to the inclusion), respectively.

the inclusion in the zoomed-in figures. The contact in large deformations is resolved without any visually-observed negative gap between the surfaces. At $u^0 = 0.3$, the matrix elements stretch to almost twice the size of the inclusion elements at the interface. The contour plot of the von Mises stress,

$$\sigma_{VM} = \sqrt{\frac{3}{2} \boldsymbol{\sigma}^d : \boldsymbol{\sigma}^d},$$

at $u^0 = 0.3$ is shown in Fig. 6a.

3.4.2. Interlocking

The second considered problem is the opening and the shear of the curved interface leading to localised deformation. Such scenario resembles the interlocking between cogs in mechanical devices. The interface is given by curve

$$X_2 = \frac{1}{2} + \frac{1}{7} \cos \left(4\pi X_1 - \frac{59\pi}{40} \right).$$

Physical parameters of the interface $\psi = 10^{-4}$, $a = 10^{-1}$ are taken. Boundary conditions (68) are used with $\bar{u}^0 = d\bar{e}_1 + 0.2\bar{e}_2$, where d is varied from 0.12 to 0.23. The deformed configuration at various d is shown in Fig. 7. It can be seen that the points that come in contact in the current configuration are significantly distanced in the reference configuration. The contact conditions are properly resolved leading to sliding of the surfaces. The contact pressure leads to bending of the curved parts of the interface. The contour plot of the von Mises stress at $d = 0.23$ is shown in Fig. 6b.

3.4.3. Crack growth

The third considered example is the crack growth problem. The aim of this example is to demonstrate one of the biggest advantages of the CutFEM technique — the interface (e.g. the crack) can evolve in time in arbitrary way

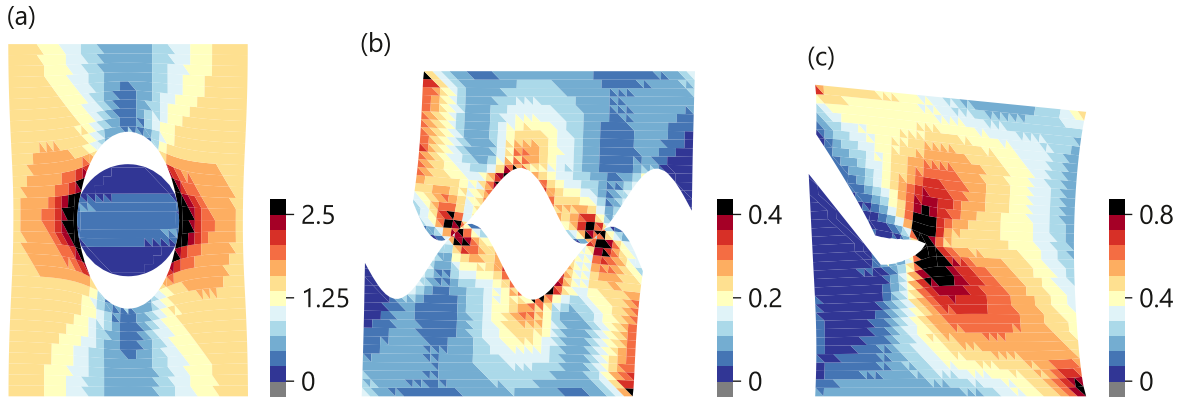


Fig. 6. The contour plots of the von Mises stress for the inclusion (a), the interlocking (b) and the crack growth (c) examples shown on the geometry of the body in the current configuration.

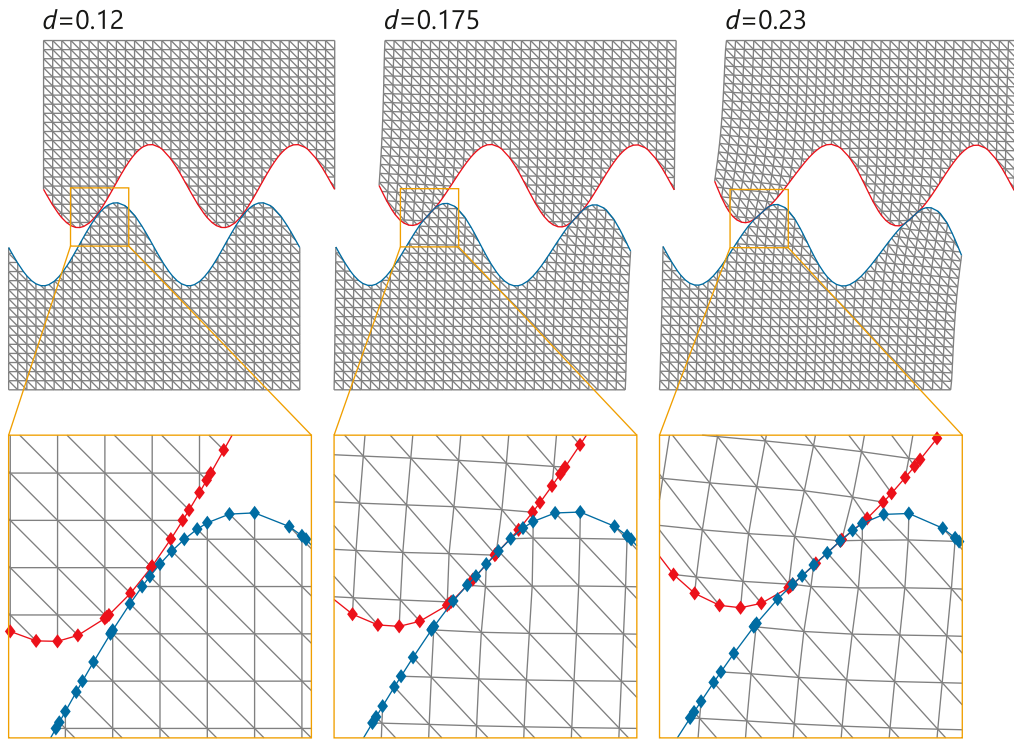


Fig. 7. The geometry of the body in the current configuration for the interlocking example. The red and the blue diamonds indicate the intersections of the element edges with surfaces γ_-^* (belonging to the upper subdomain) and γ_+^* (belonging to the lower subdomain), respectively.

from the computational point of view. Since the focus of this paper is on numerical method, very simplified physics of the crack growth is considered, which is sufficient for the demonstrative purposes; obviously, the computational method can handle more realistic crack propagation physics. Initial configuration of the interface is an inclined notch given by line $X_2 = (19 - 32X_1)/23$, $X_1 \in [0; 0.25]$. The crack tip propagates in time depending on the eigenvalues and the eigenvectors of the Cauchy stress tensor, similar to [24].

To define the propagation direction, average stress σ^A around the crack tip is introduced, calculated as the volume average within some small domain Ω_A . The highest eigenvalue of σ^A is denoted as b and the corresponding eigenvector is denoted as \vec{w} . The rotation tensor is denoted as R_\perp and the rotation angle of R_\perp is chosen to be

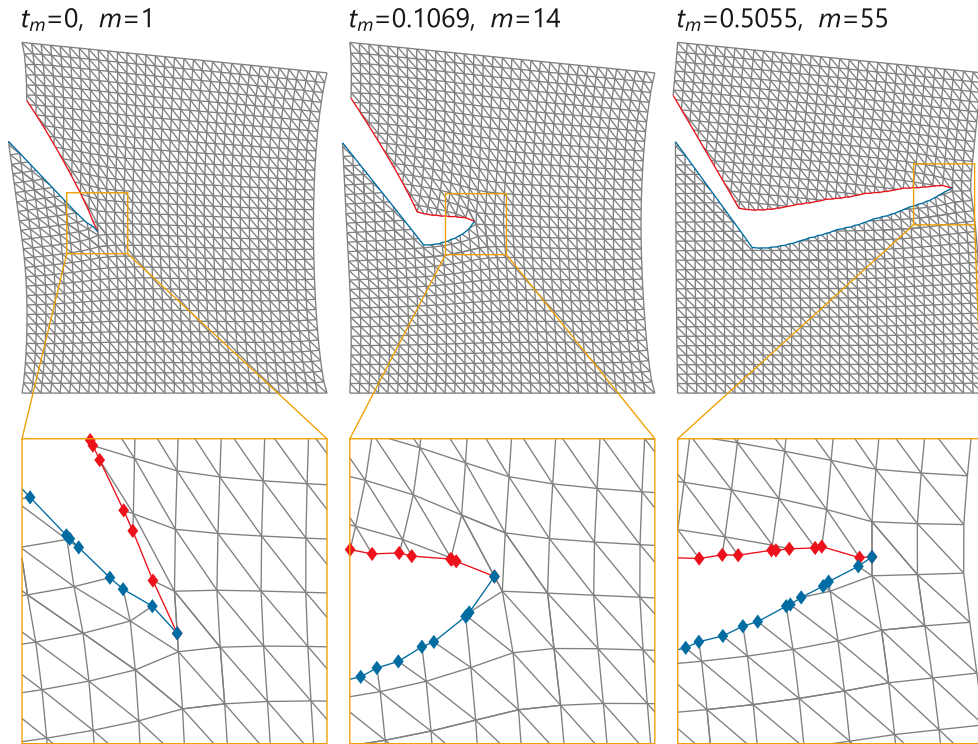


Fig. 8. The geometry of the body in the current configuration for the case of the crack growth. The red and the blue diamonds indicate the intersections of the element edges with surfaces γ_-^* and γ_+^* , respectively.

either $\pi/2$ or $3\pi/2$, such that the crack tip is not allowed to turn ‘backwards’. The velocity of the crack tip in the reference configuration is defined as

$$\vec{V} = \alpha b \frac{\mathbf{F}_{\pm}^{-1} \cdot \mathbf{R}_{\perp} \cdot \vec{w}}{|\mathbf{F}_{\pm}^{-1} \cdot \mathbf{R}_{\perp} \cdot \vec{w}|}, \tag{70}$$

where α is the kinetic constant and for the simulations $\alpha = 1$ is taken. In the numerical simulations, the crack tip is advanced using the forward Euler method. This means that given the configuration of the crack, the deformed state and the stresses are found at first. Domain Ω_A is selected as all elements that are adjacent to the nodes, which belong to the element edge, onto which the crack tip falls. Then, the velocity of the crack propagation in the reference configuration is found according to Eq. (70). The crack tip is moved along \vec{V} just until it hits the next intersection with the element edge. Since ΔX of such movement is known, the time step Δt required for the movement of the tip is calculated from the absolute value of \vec{V} .

Physical parameters of the interface $\psi = 10^{-4}$, $a = 10^{-1}$ are taken. Boundary conditions (68) are used with $\vec{u}^0 = (0.15 - 0.1X_1) \vec{e}_2$. These boundary conditions create inhomogeneous stress state and lead to the crack propagating in the direction different to the direction of the initial notch. The simulation setup can be understood as taking the stress-free geometry, creating the initial notch and instantaneously applying the boundary conditions; afterwards, the crack starts propagating. The results of the simulations are shown in Fig. 8, where the crack geometry at different iterations is illustrated. Quantity t_m shows the time corresponding to iteration number m , before the crack tip is advanced. The deformed state of the geometry at the first iteration (i.e. the crack has not propagated yet) is shown on the left. Due to high stretch of the left side of the geometry, the region below the notch significant rotates outwards. The crack then advances in the direction approximately 14° to \vec{e}_1 in the reference configuration, which also leads to a significant change of the deformed state of the geometry. The contour plot of the von Mises stress at iteration $m = 14$ is shown in Fig. 6c.

4. Conclusions

In this paper, a novel generalisation of the CutFEM approach for fracture and contact problems in large-deformation solid mechanics has been presented. Within the proposed method, the weak forms are derived from the total energy functional, which contains the interfacial energy term that is responsible for ensuring that the correct interface behaviour is obtained. Five different interfacial energy terms have been considered corresponding to five different scenarios: phase boundary, crack opening with linear and non-linear traction-separation, contact without and with adhesion.

It has been shown that each incremental generalisation of the approach contains a prior approach as a particular case. As discussed in the introduction, application of the Nitsche's method to solve the considered problems (phase boundary, crack opening, contact) has been studied extensively for the case of linear elasticity. The generalisations proposed here contain the linear elasticity as a particular case. The crack opening case generalises the phase boundary case and allows non-zero gap between the interface points. The contact without adhesion generalises the phase boundary case and allows for the interaction between the points that are not coinciding in the reference configuration, while the contact with adhesion performs a similar generalisation of the crack opening case.

Another advantage of the proposed generalisation is that for all problems, including the contact problem, the weak form is completely symmetric with respect to the choice of the surfaces for the integration, i.e. it contains integrals and quantities (e.g. deformation gradients, stresses) from both subdomains and these integrals have identical structure. For contact problems this is usually referred to as the unbiased formulation. Finally, in the resulting weak forms for the contact case, the integrals over a surface contain the finite-element test functions belonging only to that surface. This avoids projection of the test functions from one surface onto another, which is very convenient from the programming point of view leading to a shorter and a better structured code.

The proposed method has been implemented in MATLAB and tested computationally for the case of linear elements. It has passed the tests imposing homogeneous deformations ("patch tests") and the convergence rate tests. The method can be used for modelling phase boundaries (including non-stationary phase boundaries, as considered in [31]), predefined interfaces where damage is expected to take place or cracks that grow in arbitrary direction. The contact part automatically accounts for the closure of the cracks and the contact between parts of these cracks in large-deformation setting. The results of this paper might be interesting for software developers working on finite-element software and aiming to utilise the power of the CutFEM methodology in application to non-linear large-deformation solid mechanics problems.

Declaration of competing interest

The authors declare the following financial interests/personal relationships which may be considered as potential competing interests: the authors report that the financial support was provided by the European Union.

Acknowledgement

The authors acknowledge the financial support from the EU Horizon 2020 project ECO2LIB, number 875514.

Appendix. Finite-element formulation

The finite-element mesh covers the entire volume of the body $\Omega = \Omega_+ \cup \Omega_-$ and is arbitrary with respect to interface Γ_* . Without loss of generality, the mesh is considered to be conforming to the external boundary of the body, $\partial\Omega$.

The mesh contains N nodes. The standard nodal basis function associated with node i is denoted as ψ_i . These functions are continuous piecewise-polynomial functions and are equal to 1 at node i and equal to 0 at all other nodes. The space of the standard nodal basis functions is denoted as

$$\mathcal{S}^h = \text{span} \{ \psi_i \}_{i=1}^N, \quad \psi_i = \psi_i(\vec{X}).$$

To shorten the notation, additional space is introduced,

$$\mathcal{Q}^h = \{ \vec{\varphi} \mid \varphi_j \in \mathcal{S}^h \}, \quad \varphi_j = \vec{\varphi} \cdot \vec{e}_j, \quad j \in \{1, 2, 3\}.$$

Furthermore, globally defined functions $\vec{u}_+^h, \vec{u}_-^h \in \mathcal{Q}^h$ are introduced. Restrictions of functions \vec{u}_+^h and \vec{u}_-^h to domains Ω_+ and Ω_- , respectively, approximate solutions \vec{u}_+ and \vec{u}_- , respectively.

The set of all elements is denoted as \mathcal{T} . Furthermore, the following sets can be defined:

$$\mathcal{T}_\pm = \{E \mid E \in \mathcal{T}, E \cap \Omega_\pm^h \neq \emptyset\},$$

where E denotes an element. Sets \mathcal{T}_+ and \mathcal{T}_- overlap, i.e. they share the set of elements that are intersected by Γ_*^h . The set of all elements intersected by the interface is denoted as

$$\mathcal{T}_* = \mathcal{T}_+ \cap \mathcal{T}_-.$$

Here, superscript h is added to Ω_\pm and Γ_* to indicate the discretisation of the boundaries of the domains.

Thus, the finite-element formulation of the problem is the following:

$$\begin{aligned} \text{find } \vec{u}_+^h, \vec{u}_-^h \in \mathcal{Q}^h \text{ such that } & a(\vec{u}_+^h, \vec{u}_-^h, \vec{\varphi}_+^h, \vec{\varphi}_-^h) = 0, \quad \forall \vec{\varphi}_+^h, \vec{\varphi}_-^h \in \mathcal{Q}^h, \\ \vec{u}_\pm^h &= \vec{0} \text{ at nodes that do not belong to elements } \mathcal{T}_\pm, \\ \vec{u}_\pm^h &= \vec{d} \text{ at nodes on } \Gamma_D \cap \mathcal{T}_\pm, \end{aligned}$$

where functional a was defined in (12). The above finite-element problem represents a system of non-linear algebraic equations with respect to nodal values of \vec{u}_+^h and \vec{u}_-^h , which can be solved using the standard Newton–Raphson method.

References

- [1] E. Burman, P. Hansbo, Fictitious domain finite element methods using cut elements: II. A stabilized Nitsche method, *Appl. Numer. Math.* 62 (4) (2012) 328–341.
- [2] E. Burman, S. Claus, P. Hansbo, M.G. Larson, A. Massing, CutFEM: Discretizing geometry and partial differential equations, *Internat. J. Numer. Methods Engrg.* 104 (7) (2015) 472–501.
- [3] A. Hansbo, P. Hansbo, An unfitted finite element method, based on Nitsche’s method, for elliptic interface problems, *Comput. Methods Appl. Mech. Engrg.* 191 (2002) 5537–5552.
- [4] J. Nitsche, Über ein variationsprinzip zur lösung von Dirichlet-problemen bei verwendung von teilträumen, die keinen randbedingungen unterworfen sind, *Abh. Math. Semin. Univ. Hambg.* 36 (1) (1971) 9–15.
- [5] E. Burman, P. Hansbo, M.G. Larson, A cut finite element method with boundary value correction, *Math. Comp.* 87 (310) (2018) 633–657.
- [6] E. Burman, P. Hansbo, M.G. Larson, A. Massing, Cut finite element methods for partial differential equations on embedded manifolds of arbitrary codimensions, *ESAIM Math. Model. Numer. Anal.* 52 (6) (2018) 2247–2282.
- [7] E. Burman, P. Hansbo, M.G. Larson, S. Zahedi, Stabilized CutFEM for the convection problem on surfaces, *Numer. Math.* 141 (1) (2019) 103–139.
- [8] E. Burman, P. Hansbo, M.G. Larson, A. Massing, A stable cut finite element method for partial differential equations on surfaces: The Helmholtz–Beltrami operator, *Comput. Methods Appl. Mech. Engrg.* 362 (2020) 112803.
- [9] M.G. Larson, S. Zahedi, Stabilization of high order cut finite element methods on surfaces, *IMA J. Numer. Anal.* 40 (3) (2020) 1702–1745.
- [10] P. Hansbo, M.G. Larson, S. Zahedi, A cut finite element method for coupled bulk-surface problems on time-dependent domains, *Comput. Methods Appl. Mech. Engrg.* 307 (2016) 96–116.
- [11] S. Zahedi, A space-time cut finite element method with quadrature in time, in: S.P.A. Bordas, E. Burman, M.G. Larson, M.A. Olshanskii (Eds.), *Geometrically Unfitted Finite Element Methods and Applications*, Springer International Publishing, 2017, pp. 281–306.
- [12] E. Burman, D. Elfverson, P. Hansbo, M.G. Larson, K. Larsson, Shape optimization using the cut finite element method, *Comput. Methods Appl. Mech. Engrg.* 328 (2018) 242–261.
- [13] E. Burman, D. Elfverson, P. Hansbo, M.G. Larson, K. Larsson, Cut topology optimization for linear elasticity with coupling to parametric nondesign domain regions, *Comput. Methods Appl. Mech. Engrg.* 350 (2019) 462–479.
- [14] T. Belytschko, T. Black, Elastic crack growth in finite elements with minimal remeshing, *Internat. J. Numer. Methods Engrg.* 45 (5) (1999) 601–620.
- [15] N. Moës, J. Dolbow, T. Belytschko, A finite element method for crack growth without remeshing, *Internat. J. Numer. Methods Engrg.* 46 (1) (1999) 131–150.
- [16] T. Belytschko, R. Gracie, G. Ventura, A review of extended/generalized finite element methods for material modeling, *Modelling Simulation Mater. Sci. Eng.* 17 (4) (2009) 043001.
- [17] J.M. Melenk, I. Babuska, The partition of unity finite element method: Basic theory and applications, *Comput. Methods Appl. Mech. Engrg.* 139 (1–4) (1996) 289–314.
- [18] T. Rabczuk, J.-H. Song, X. Zhuang, C. Anitescu, *Extended Finite Element and Meshfree Methods*, Academic Press, 2019.
- [19] Y. Krongauz, T. Belytschko, EFG approximation with discontinuous derivatives, *Internat. J. Numer. Methods Engrg.* 41 (7) (1998) 1215–1233.

- [20] T. Belytschko, N. Moës, S. Usui, C. Parimi, Arbitrary discontinuities in finite elements, *Internat. J. Numer. Methods Engrg.* 50 (4) (2001) 993–1013.
- [21] N. Sukumar, D.L. Chopp, N. Moës, T. Belytschko, Modeling holes and inclusions by level sets in the extended finite-element method, *Comput. Methods Appl. Mech. Engrg.* 190 (46–47) (2001) 6183–6200.
- [22] H. Ji, J.E. Dolbow, On strategies for enforcing interfacial constraints and evaluating jump conditions with the extended finite element method, *Internat. J. Numer. Methods Engrg.* 61 (14) (2004) 2508–2535.
- [23] H.M. Mourad, J. Dolbow, I. Harari, A bubble-stabilized finite element method for Dirichlet constraints on embedded interfaces, *Internat. J. Numer. Methods Engrg.* 69 (4) (2007) 772–793.
- [24] A. Hansbo, P. Hansbo, A finite element method for the simulation of strong and weak discontinuities in solid mechanics, *Comput. Methods Appl. Mech. Engrg.* 193 (33–35) (2004) 3523–3540.
- [25] G.N. Wells, L.J. Sluys, A new method for modelling cohesive cracks using finite elements, *Internat. J. Numer. Methods Engrg.* 50 (12) (2001) 2667–2682.
- [26] N. Moës, T. Belytschko, Extended finite element method for cohesive crack growth, *Eng. Fract. Mech.* 69 (7) (2002) 813–833.
- [27] T. Belytschko, H. Chen, J.X. Xu, G. Zi, Dynamic crack propagation based on loss of hyperbolicity and a new discontinuous enrichment, *Internat. J. Numer. Methods Engrg.* 58 (12) (2003) 1873–1905.
- [28] S. Mariani, U. Perego, Extended finite element method for quasi-brittle fracture, *Internat. J. Numer. Methods Engrg.* 58 (1) (2003) 103–126.
- [29] P. Hansbo, M.G. Larson, K. Larsson, Cut finite element methods for linear elasticity problems, in: S.P.A. Bordas, E. Burman, M.G. Larson, M.A. Olshanskii (Eds.), *Geometrically Unfitted Finite Element Methods and Applications*, Springer International Publishing, 2017, pp. 25–63.
- [30] P. Hansbo, Nitsche’s method for interface problems in computational mechanics, *GAMM-Mitt.* 28 (2) (2005) 183–206.
- [31] M. Poluektov, L. Figiel, A numerical method for finite-strain mechanochemistry with localised chemical reactions treated using a Nitsche approach, *Comput. Mech.* 63 (5) (2019) 885–911.
- [32] P. Wriggers, G. Zavarise, A formulation for frictionless contact problems using a weak form introduced by Nitsche, *Comput. Mech.* 41 (3) (2008) 407–420.
- [33] R. Mlika, Y. Renard, F. Chouly, An unbiased Nitsche’s formulation of large deformation frictional contact and self-contact, *Comput. Methods Appl. Mech. Engrg.* 325 (2017) 265–288.
- [34] F. Chouly, P. Hild, A Nitsche-based method for unilateral contact problems: Numerical analysis, *SIAM J. Numer. Anal.* 51 (2) (2013) 1295–1307.
- [35] F. Chouly, P. Hild, Y. Renard, Symmetric and non-symmetric variants of Nitsche’s method for contact problems in elasticity: Theory and numerical experiments, *Math. Comp.* 84 (293) (2015) 1089–1112.
- [36] A. Seitz, W.A. Wall, A. Popp, Nitsche’s method for finite deformation thermomechanical contact problems, *Comput. Mech.* 63 (6) (2019) 1091–1110.
- [37] E. Burman, P. Hansbo, Deriving robust unfitted finite element methods from augmented Lagrangian formulations, in: S.P.A. Bordas, E. Burman, M.G. Larson, M.A. Olshanskii (Eds.), *Geometrically Unfitted Finite Element Methods and Applications*, Springer International Publishing, 2017, pp. 1–24.
- [38] M.J. van den Bosch, P.J.G. Schreurs, M.G.D. Geers, On the development of a 3D cohesive zone element in the presence of large deformations, *Comput. Mech.* 42 (2) (2008) 171–180.
- [39] S. Claus, P. Kerfriden, A stable and optimally convergent LaTIn-CutFEM algorithm for multiple unilateral contact problems, *Internat. J. Numer. Methods Engrg.* 113 (6) (2018) 938–966.
- [40] H. Kothari, R. Krause, Multigrid and saddle-point preconditioners for unfitted finite element modelling of inclusions, in: F. Chinesta, R. Abgrall, O. Allix, M. Kaliske (Eds.), *WCCM-ECCOMAS2020*, 2020, pp. 1–12.
- [41] H. Kothari, R. Krause, A generalized multigrid method for solving contact problems in Lagrange multiplier based unfitted finite element method, 2021, Preprint [arXiv:2106.16107v1](https://arxiv.org/abs/2106.16107v1).
- [42] R.W. Ogden, Large deformation isotropic elasticity: On the correlation of theory and experiment for compressible rubberlike solids, *Proc. R. Soc. A* 328 (1575) (1972) 567–583.
- [43] C.O. Horgan, G. Saccomandi, Constitutive models for compressible nonlinearly elastic materials with limiting chain extensibility, *J. Elasticity* 77 (2) (2004) 123–138.